Antimicrobial Agents and Chemotherapy

Research Article

Nodosome inhibition as a novel broad-spectrum antiviral strategy against arboviruses and SARS-CoV-2

Daniel Limonta,[a,b] Lovely Dyna-Dagman,[c] William Branton,[d] Tadashi Makio,[a] Richard W. Wozniak,[a, b] Christopher Power,[c,d,e] Tom C. Hobman[a,b,c,e] #

[a] Department of Cell Biology, University of Alberta, Edmonton, Canada

[b] Li Ka Shing Institute of Virology, University of Alberta, Edmonton, Canada

[c] Department of Medical Microbiology & Immunology, University of Alberta, Edmonton, Canada

[d] Department of Medicine, University of Alberta, Edmonton, Canada

[e] Women & Children's Health Research Institute, University of Alberta, Edmonton, Canada

Running Head: Nodosome inhibition as novel antiviral strategy

Address correspondence to Tom C. Hobman, tom.hobman@ualberta.ca.

ABSTRACT

In the present report, we describe two small molecules with broad-spectrum antiviral activity. These drugs block formation of the nodosome. The studies were prompted by the observation that infection of human fetal brain cells with Zika virus (ZIKV) induces expression of nucleotide-binding oligomerization domain-containing protein 2 (NOD2), a host factor that was found to promote ZIKV replication and spread. A drug that targets NOD2 was shown to have potent broad-spectrum antiviral activity against other flaviviruses, alphaviruses and SARS-CoV-2, the causative agent of COVID-19. Another drug that inhibits the receptor-interacting serine/threonine-protein kinase 2 (RIPK2) which functions downstream of NOD2, also decreased replication of these pathogenic RNA viruses. The broad-spectrum action of nodosome targeting drugs is mediated, at least in part, by enhancement of the interferon response. Together, these results suggest that further preclinical investigation of nodosome inhibitors as potential broad-spectrum antivirals is warranted.

KEYWORDS antiviral, broad-spectrum, NOD2, RIPK2, arbovirus, SARS-CoV-2, COVID-19, nodosome, interferon

INTRODUCTION

Re-emerging and emerging RNA viruses represent a major threat to global public health. Vaccines and antiviral drugs which usually target a single virus species, are critical measures to prevent and control the spread of these pathogens. However, prophylactic or therapeutic drugs are not available for many of the most important RNA viruses in circulation today (1). While highly effective direct-acting antiviral drugs have been developed for a number of important human pathogens such as HIV-1, herpesvirus family members and hepatitis C virus (2), these drugs tend to be highly specific and are of limited use for treating other viral infections. In contrast, broad-spectrum antivirals would be expected to inhibit replication of multiple viruses, including emerging and re-emerging RNA viruses. Although several broad-spectrum antiviral compounds are in preclinical studies or in clinical trials, to date, no drug in this class has been licensed (3). Because hundreds of cellular factors are required for productive viral infection, targeting common host factors that are utilized by multiple viruses, may be a viable approach for developing broad-spectrum antivirals (4).

Herein we report the identification and characterization of a novel class of small molecules with broad-spectrum antiviral activity. These drugs selectively block the intracellular pattern recognition receptor NOD2 (nucleotide-binding oligomerization domain-containing protein 2), and a critical mediator of NOD2 signalling, RIPK2 (receptor-interacting serine/threonine-protein kinase 2). NOD2 recognizes the peptidoglycan muramyl dipeptide (MDP) that is found in bacterial cell walls, but it can also bind to viral RNA. In doing so, NOD2 induces formation of the nodosome and stimulates host defense against infections (5). Although NOD2 is important for the innate immune response against HIV-1 (6), cytomegalovirus (7) and syncytial respiratory virus (8), it has also been reported as a major pathogenic mediator of coxsackievirus B3-induced myocarditis (9).

Previously, we reported that Zika virus (ZIKV) infection of human fetal brain cells upregulates the expression of NOD2 (10) and here, we show that expression of this host protein promotes ZIKV replication. Using multiple human primary cell types, tissue explants, and cell lines, we found that the NOD2 blocking drug, GSK717, inhibits replication of flaviviruses, alphaviruses and SARS-CoV-2, the causative agent of COVID-19. The broad-spectrum activity of this drug is mediated in part by enhancement of the innate immune response. The RIPK2 blocking agent, GSK583, also potently inhibits these pathogenic RNA viruses. Together, data from our *in vitro* and *ex vivo* experiments suggest that nodosome inhibitors should be further investigated as broad-spectrum antivirals in preclinical studies.

RESULTS

ZIKV infection induces the inflammasome in primary human fetal brain cells

Previously, we reported that HFAs are likely the principal reservoirs for ZIKV infection and persistence in the human fetal brain (11). In a subsequent study (10), RNAseq analyses revealed that ZIKV infection of these cells upregulates multiple inflammasome genes including *GSDMD*, *IL-1 β, Casp1, NLRC5, GBP5,* and *NOD2*. In light of the recently identified links between the inflammasome and ZIKV neuropathogenesis (12, 13), we asked whether the activity of this multiprotein complex affected virus replication. Since our previous analysis (10) was performed using a strain of ZIKV not associated with microcephaly, we first confirmed that infection of HFAs with the pandemic ZIKV strain PRVABC-59 induced expression of multiple inflammasome genes. Indeed, *NOD2* and *GBP5* were upregulated more than 100-fold by ZIKV infection whereas other genes in this pathway were induced less than 50-fold (Fig. 1 A). Expression of inflammasome genes could also be induced by treatment of HFAs with human recombinant IFN-α, but less so

than with the double-strand RNA mimic poly(I:C) (Fig. 1 B and C, Fig. S1 A-D). This may indicate that detection of viral RNA *per se* triggers inflammasome induction.

NOD2 expression promotes ZIKV multiplication by suppression of the innate immune response in HFAs

As *NOD2* was one of the most upregulated inflammasome genes, we examined how reduced NOD2 expression in HFAs affected replication of the PRVABC-59 strain of ZIKV. Compared to cells transfected with a non-targeting siRNA, replication of ZIKV in HFAs transfected with NOD2-specific siRNAs was significantly reduced (Fig. 2 A and B).

Recently, we reported that ZIKV-induced expression of fibroblast growth factor 2 in fetal brain increases viral replication by inhibiting the interferon response (10). As NOD2 is an intracellular pattern recognition receptor that recognizes bacterial MDP as well as viral RNA (5), we questioned whether the effect of NOD2 expression on viral replication was related to its actions on the innate immune response. To address this, relative expression of ISGs was determined in ZIKV-infected HFAs after *NOD2* silencing. *NOD2* knockdown was associated with significant upregulation of several important ISGs including *Viperin*, *OAS1*, and *MX2* (Fig. 2 C) as well as the prototypic inflammasome genes *GSDMD* and *Casp1* (Fig. 2 D). Of note, *NOD2* silencing reduced *NOD2* mRNA expression and was not cytotoxic for HFAs (Fig. S1 E and F).

ZIKV replication and spread are inhibited by blocking NOD2 function in fetal brain

A number of specific NOD2 inhibitors have been developed to treat inflammatory diseases (14). To determine if these drugs have antiviral activity, HFAs infected with ZIKV were treated with or without subcytotoxic concentrations of the anti-NOD2 compound, GSK717, for up to 72 hours.

GSK717 reduced viral titers in a concentration-dependent manner regardless of whether cells were infected at low or high MOI (Fig. 3 A and B).

We also investigated whether GSK717 could block ZIKV replication in explanted human fetal brain tissue as described previously (15). Data in Fig. 3 C-E show that GSK717 treatment significantly inhibited replication of viral genomic RNA and reduced viral titers of ZIKV by as much as 33-fold. Similar results were observed in human primary embryonic pulmonary fibroblasts (HEL-18) thus demonstrating that the antiviral effect of GSK717 is not limited to fetal brain tissue (Fig. S2 A-C).

NOD2 inhibitor blocks ZIKV infection and spread in multiple cell lines

We next examined whether GSK717 also inhibits ZIKV replication in human non-prenatal cell types, including cell lines usually used for anti-flavivirus drug screening such as A549 (pulmonary) and Huh7 (hepatoma) cells (16) as well as the astrocytoma cell line U251. GSK717 significantly reduced ZIKV titers in these human cell lines in a dose-dependent manner regardless of whether low (0.05) and high (5) MOI were used for infection (Fig. S2 D-F). GSK717 also showed a concentration-dependent inhibitory effect on ZIKV replication in mouse embryonic fibroblasts (data not shown). Consistent with its ability to reduce viral titers, treatment with GSK717 significantly reduced the numbers of infected cells in A549 cultures (Fig. 4 A and B). Interestingly, GSK717 inhibited ZIKV replication even when added 12- or 24-hours post-infection (Fig. S2 G). None of the GSK717 concentrations used in the cell-based assays were cytotoxic at the examined time points (Fig. S3).

DENV replication is inhibited by the anti-NOD2 drug GSK717

To determine if GSK717 could inhibit replication of other flaviviruses, we next focused on DENV, the most important arbovirus in terms of morbidity and mortality and the causative agent of Dengue Hemorrhagic Fever/Dengue Shock Syndrome (17). A549 cells infected with DENV-2 strain 16681 (18) were treated with or without increasing concentrations of GSK717. Data in Fig. 5 A-C show that GSK717 reduced DENV titers by >90% when used at 20-40 μM. Blocking NOD2 function with GSK717 also dramatically reduced the number of viral antigen positive-A549 cells after 48 hours of infection (Fig. S4 A and B).

Finally, as co-infections of DENV-2 with ZIKV have been reported in Latin American (19, 20) and South Asian countries (21), we assessed how GSK717 affected virus replication in A549 simultaneously infected with ZIKV and DENV-2. Results from qRT-PCR analyses revealed that levels of both ZIKV and DENV genomic RNA were reduced by ~60% in GSK717-treated cells (Fig. 5 D and E).

NOD2 function is important for replication of alphaviruses and coronaviruses

Nodosome formation can be induced following infection by multiple types of RNA viruses (22). As such, we next determined whether GSK717 could inhibit replication of the mosquito-transmitted alphavirus, MAYV. The recent outbreak strain TRVL 15537 MAYV was used for these experiments. Supernatants from infected A549 cell cultures treated with or without GSK717 were collected for viral titer determination at 48-hours post-infection after which plaque assays were performed. Similar to what was observed in flavivirus-infected cells, we found that GSK717 reduced MAYV titers by as much as 95% (Fig. 6 A and B). MAYV and DENV-2 co-circulate in the same areas of South America and dual infections have been reported recently (23). Treatment of co-infected A549 cells with GSK717 resulted in significant inhibition of both DENV-2 and MAYV although replication of the latter was affected to a larger degree (Fig. 6 C and D).

Because SARS-CoV-2 infection reportedly activates the inflammasome *in vitro* (24) and in patients (25, 26), we tested how NOD2 inhibition affected replication of this pandemic coronavirus. A neuroblastoma cell line (SK-N-SH) stably expressing ACE2 was infected with a Canadian isolate of SARS-CoV-2 and treated with or without GSK717. At 48-hours post-infection, culture supernatants were collected for viral titer determination by plaque assay using Vero-E6 cells. Data in Fig. 6 E and F show that pharmacological inhibition of NOD2 resulted in reduction of SARS-CoV-2 titers similar to what was observed with arboviruses.

Inhibition of downstream RIPK2 supresses replication of multiple RNA viruses including SARS-CoV-2

RIPK2 is a critical mediator of NOD2 signalling. Binding of MDP to NOD2 leads to self-oligomerization of NOD2 molecules, followed by homotypic interactions between the C-terminal caspase activation and recruitment domain of NOD2 and RIPK2. This results in the activation of transcription factors that drive the expression of multiple proinflammatory cytokines, chemokines and anti-bacterial proteins (27).

Although RIPK2 mRNA was not upregulated in ZIKV infected-HFAs (10), we questioned whether pharmacological inhibition of this protein would also reduce replication of arboviruses such ZIKV, DENV-2 and MAYV. Infected A549 cells were treated with or without GSK583, a highly potent and selective inhibitor of the NOD2 binding domain of RIPK2 (28). Significant reduction in viral titers was observed in GSK583-treated cells infected with ZIKV, DENV-2 or MAYV at 12- and 24-hours post-infection (Fig. 7 A-C, Fig. S5 A-D). The antiviral action of GSK583 was corroborated in another human cell line, Huh7, infected with MAYV (MOI=0.1) (data not shown).

Similarly, indirect immunofluorescence microscopy analyses confirmed that inhibition of RIPK2 reduced the number of viral antigen-positive cells in ZIKV, DENV-2 and MAYV-infected A549 cultures (Fig. S6 A-D).

We tested the effect of GSK583 on replication of SARS-CoV-2 in ACE2-SK-N-SK cells. At 12 and 24-hours post-infection, culture supernatants and cell lysates were collected for viral titer determination by plaque assay and viral ARN quantification using qRT-PCR. A significant concentration-dependent reduction in viral multiplication was observed in GSK583-treated cells (Fig. 7 D-F and Fig. S7 A). A time-of-addition assay (drug treatment at 0- and 24-hour post-infection) demonstrated that the RIPK2 inhibitor was able to reduce virus replication even when the drug was added well after viral infection had occurred (Fig. S7 B). Quantitation of infection by indirect immunofluorescence showed that GSK583 treatment reduced the numbers of infected cells in a monolayer culture (Fig. S7 C and D).

Finally, when RIPK2 inhibition experiments were conducted using Calu-3 and Huh7 cells for 24 hours, ~60% and ~90% reduction in titers respectively were observed with the highest concentration of RIPK2 inhibitor (Fig. S8 A and B). No cytotoxic effect of GSK583 were detected in the cell lines used for coronavirus assays (Fig. S8 C-E).

DISCUSSION

ZIKV co-circulates in some of the same endemic regions as other arboviruses including chikungunya virus, DENV, and MAYV. Symptoms of acute infection caused by these arboviruses such as fever, rash, joint pain, and ocular manifestations are common which complicates clinical diagnosis of mono- and co-infections (17, 29, 30). Differential serological diagnosis is further hindered by flavivirus antigen cross-reactivity (17, 30). Given the issues with clinical/laboratory

diagnosis and lack of effective vaccines against most arboviruses, development of broad-spectrum antivirals against these pathogens should be a high priority.

The ongoing pandemic caused by SARS-CoV-2 poses a different set of challenges. Despite concerted efforts to repurpose and find new antiviral drugs (31-33), so far only remdesivir has shown modest efficacy in the acute stages of COVID-19 (34, 35). While more than 200 SARS-CoV-2 vaccine candidates are in accelerated development at preclinical and clinical stages (36), it will likely take another year or more before they are broadly available to the general population as safety and efficacy still need to be evaluated (37, 38).

In this study, we characterized the broad-spectrum antiviral activities of nodosome inhibitors GSK717 and GSK583. These small molecules display robust antiviral action against multiple RNA viruses and may hold promise as pan-flavivirus inhibitors. First, we showed that NOD2 expression promotes ZIKV multiplication in HFAs which are the main target of this flavivirus in the fetal brain (10, 11). Next, we demonstrated that the NOD2 inhibitor GSK717 blocks infection by and spread of ZIKV in human fetal brain and cell lines. NOD2 inhibition also reduced replication of the related DENV, the alphavirus MAYV and the pandemic coronavirus SARS-CoV-2. Blocking the NOD2 downstream signaling kinase RIPK2 with GSK583 (which does not affect its catalytic activity) significantly inhibited replication of these viral pathogens.

Gefitinib is an FDA-approved drug for treatment of lung, breast and other cancers. It works by reducing the activity of the epidermal growth factor receptor (EGFR) tyrosine kinase domains. Of note, this drug also inhibits the tyrosine kinase activity of RIPK2 (39) and has been shown to inhibit replication of DENV and release of pro-inflammatory cytokines from infected human primary monocytes (40). The authors suggested a role for EGFR/RIPK2 in DENV pathogenesis and that gefitinib may be beneficial in the treatment of dengue patients. Similarly, the work here

which demonstrated the antiviral activity of NOD2 and RIPK2 inhibitors using tissue explants, primary cells and cell lines, support the potential clinical use of these compounds in mono or co-infections by arboviruses as well as coronavirus infections at early and/or advanced stages.

As GSK717 and GSK583 were developed primarily for immune-mediated inflammatory conditions, their anti-inflammatory effects may have the added benefit of reducing the hyperinflammatory state associated with flavi-, alpha- and coronavirus diseases (17, 29, 30, 41). Finally, our findings raise potential concerns regarding adjuvants in viral vaccines that augment NOD2 as an immune strategy (42, 43) since this immune signaling protein is not a restriction factor but rather an enhancement factor for multiple pathogenic RNA viruses.

The current study illustrates how the identification of a drug target through transcriptomic analyses of virus-infected cells can lead to novel broad-acting host-directed antiviral strategies with a high barrier of resistance. Increased NOD2 expression may be a novel mechanism of immune evasion that viruses use to evade the innate immune response. Conversely, drugs that block nodosome formation appear to have broad-spectrum antiviral activity by enhancing the interferon response. Collectively, our results warrant consideration of these and related compounds as broad-spectrum antiviral drug candidates for further preclinical development.

MATERIALS AND METHODS

Ethical Approval. Human fetal brain tissues were obtained from 15-19-week aborted fetuses with written consent from the donor parents and prior approval under protocol 1420 (University of Alberta Human Research Ethics Board).

Cells, explant cultures and viruses. ZIKV (PRVABC-59), Dengue virus (DENV-2, 16681), and Mayaro virus (MAYV, TRVL 15537) were propagated in *Aedes albopictus* C6/36 cells grown in

Minimum Essential Medium (MEM, Thermo Fisher Scientific, Waltham, MA). SARS-CoV-2 (SARS-CoV-2/CANADA/VIDO 01/2020) was propagated in Vero-E6 cells grown in Dulbecco's Modified Eagle Medium (DMEM, Thermo Fisher Scientific). A549, Huh7, U251, Vero (ATCC, Manassas, VA) and ACE2-hyperexpressing SK-N-SH cells were maintained in DMEM while HEL-18 human primary embryonic pulmonary fibroblasts and Calu-3 cells (ATCC) were maintained in Roswell Park Memorial Institute 1640 medium (RPMI, Thermo Fisher Scientific) and MEM respectively. Human fetal astrocytes (HFAs) and fetal brain tissue explants were prepared from multiple donations (n=8), as described previously (15). For infection, cells or tissue explants were incubated with virus (MOI 0.05-5) for 1-2 hr or overnight respectively at 37°C using fresh media supplemented with fetal bovine serum (Thermo Fisher Scientific). For co-infection assays, A549 cells were infected simultaneously with DENV-2 and ZIKV or MAYV at an MOI of 0.1 for 3 hours. Culture of cells, tissue explants, construction of the ACE2-SK-N-SH cells, and viral infections are described in more detail in Supplemental Material.

qRT-PCR. RNA from cells and tissue was extracted using NucleoSpin RNA (Macherey-Nagel GmbH & Co, Düren, Germany) kits. Real-time qRT-PCR was performed in a CFX96 Touch Real-Time PCR Detection System instrument (Bio-Rad, Hercules, CA) using ImProm-II Reverse Transcriptase (Promega, Madison, WI). For more details about the protocols, and primers used in this work please see Supplemental Material.

Poly(I:C) transfection. HFAs grown in 96-well plates (Greiner, Kremsmünster, Austria) were transfected with polyinosinic:polycytidylic acid (Poly(I:C) (Sigma-Aldrich, St. Louis, MO) at a concentration of 0.02 or 0.1 μg/well using TransIT (0.3 μL/well, Mirus Bio LLC, Madison, WI). At 12 hours post-transfection, total RNA was extracted and transcripts levels for IFN-stimulated genes (ISGs) were quantified by qRT-PCR.

Human recombinant INF-α assay. HFAs in 96-well plates (Greiner) were treated with or without 25-100 U/mL of human recombinant IFN-α (Sigma-Aldrich) for 4-12 hours after which total RNA was isolated and subjected to qRT-PCR in order to measure expression of ISGs.

Viral titer assay. Titers were determined in Vero CCL-81 and Vero-E6 for arboviruses (flaviviruses and alphaviruses) and coronaviruses respectively. Supplemental Material provides a more detailed description of the assay.

NOD2 silencing. Cells were seeded in 96-well plates (Greiner) overnight before transfection with 20 nM of NOD2 DsiRNA hs.Ri.NOD2.13.2 from Integrated DNA Technologies (IDT, Coralville, IA) using 0.3 µg/well RNAiMax (Invitrogen, Waltham, MA). The non-targeting IDT control DsiRNA was used as negative control for transfection. Twenty-four hours later, cells were infected with ZIKV using MOI of 0.05. At 24 and 48-hours post-infection, culture supernatants were collected for plaque assay. Total RNA isolated from cells at 48-hours post-infection was subjected to qRT-PCR to determine levels of viral genomic RNA and ISGs.

Measurement of cell viability. Cell viability assays in response to drug or DMSO treatment were performed using CellTiter-Glo Luminescent Cell Viability kit (Promega) in cells grown in 96-well plates (Greiner) as described in the Supplemental Material.

***In vitro* and *ex vivo* drug assays.** After drug or DMSO treatment, viral replication and titers were determined by qRT-PCR on total RNA extracted from cells or tissues and plaque assay of culture supernatants respectively 12 to 72-hours post-infection. Cells seeded into 96-well plates (Greiner) were infected with ZIKV, DENV-2, MAYV or SARS-CoV-2 (MOI=0.05-5) followed by treatment with 5, 10, 20 and 40 µM GSK717 (14) (Sigma-Aldrich) or DMSO.

Fetal brain tissue explants were treated after ZIKV infection with GSK717 (20-40 µM) or DMSO for 3 days. Viral titer determination in culture supernatants daily and viral genome quantification in tissues at 72 hours post-infection were performed.

A549 or ACE2-SK-N-SH cells on coverslips in 12-well plates (Greiner) were infected (MOI of 1.0) with arboviruses (ZIKV, DENV-2 or MAYV) or SARS-CoV2 respectively and then processed for indirect immunofluorescence. Arbovirus co-infection assays and time-of-addition assays were conducted in A549 cells while SARS-CoV-2 time-of-addition assays were performed in ACE2-SK-N-SH using an MOI of 0.1. Viral genome quantification and viral titer determination were performed in the co-infection and time-of-addition assays, respectively.

A549 cells infected with arboviruses or ACE2-SK-N-SH cells infected with SARS-CoV-2 (MOI=0.05-5) were treated with the RIPK2 inhibitor GSK583 (28) (Sigma-Aldrich) for 24 hours. Cell supernatants and total cellular RNA were collected for determining viral titers and viral RNA respectively. Please, see Supplemental Material for additional information about the drug assays.

Immunofluorescence staining and cell imaging. Infected cells grown on coverslips were fixed with 4% paraformaldehyde and permeabilized/blocked with a Triton-X100 (0.2%)/BSA (3%) solution and then incubated with mouse anti-Flavivirus Group Antigen 4G2 (Millipore, Burlington, MA), mouse anti-alphavirus capsid (kindly provided by Dr. Andres Merits at University of Tartu), or mouse anti-spike SARS-CoV/SARS-CoV-2 (GenTex, Irvine, CA) at room temperature for 1.5 hour, washed and then incubated with Alexa Fluor secondary antibodies against mouse and DAPI for 1 hour at room temperature. Antibodies were diluted in Blocking buffer. PBS containing 0.3% BSA was used for wash steps. Samples were examined using an Olympus 1x81 spinning disk confocal microscope (Tokyo, Japan) or Cytation 5 Cell Imaging

Multi-Mode Reader instrument (Biotek, Winooski, VT). Images were analyzed using Volocity or Gen5 software. More experimental details are provided in the Supplemental Material.

Statistical analyses. A paired Student's t-test was used for pair-wise statistical comparison. The standard error of the mean is shown in all bar graphs. GraphPad Prism software 5.0 (GraphPad Software Inc., La Jolla, CA) was used in all statistical analyses.

ACKNOWLEDGEMENTS

This work was supported by grants from the Canadian Institutes of Health Research (grants PJT-148699, OV3-172302, PJT-162417) and the Li Ka Shing Institute of Virology to T. C. H. The funders had no role in study design, data collection and interpretation, or the decision to submit the work for publication.

We wish to thank Dr. Anil Kumar, Dr. Joaquin Lopez Orozco, Dr. Adriana Airo, Dr. Zaikun Xu, Cheung Pang Wong, and Ray Ishida in the Hobman lab for helpful discussions and support. Confocal imaging was performed at the Cell Imaging Centre core in the Faculty of Medicine & Dentistry of the University of Alberta. We thank Dr. Darryl Falzarano (Vaccine and Infectious Disease Organization-International Vaccine Centre, University of Saskatchewan, Canada) for providing the Canadian SARS-CoV-2 strain for this work, Dr. David Safronetz (Public Health Agency of Canada, Canada) for providing the ZIKV strain, Dr. Bart Bartenschlager (Heidelberg University Hospital, Germany) for donating the DENV-2 clone, Dr. Eva Gönczöl (The Wistar Institute, USA) for providing the HEL-18 cells, and Dr. Andres Merits (University of Tartu, Estonia) for kindly donating the anti-alphavirus capsid antibody. Furthermore, we thank Eileen Reklow and Valeria Mancinelli for excellent technical support.

We declare no competing financial interests.

Figure legends

Fig. 1. Inflammasome gene expression in HFAs is induced by ZIKV, IFN-α and Poly(I:C). (**A**) Relative inflammasome gene expression in HFAs infected with PRVABC-59 ZIKV (MOI=0.3) was determined by qRT-PCR 48-hours post-infection. (**B**) HFAs were treated with human recombinant IFN-α for 4, 8 and 12 hours after which relative *NOD2* expression was determined. (**C**) HFAs were transfected with Poly(I:C) for 12 hours after which relative inflammasome gene expression was determined. Error bars represent standard errors of the mean. $*P < 0.05$, $**P < 0.01$, and $***P < 0.001$, by the Student *t* test.

Fig. 2. NOD2 silencing suppresses ZIKV multiplication and enhances the expression of interferon-stimulated and inflammasome genes. HFAs were transfected with NOD2-specific or non-silencing siRNAs for 24-hours and then infected with ZIKV (MOI=0.05). Cell culture media or total cellular RNA were harvested after 24- and 48-hours for plaque assay (**A**) or qRT-PCR at 48-hours post-infection. Relative levels of viral genome (**B**), and interferon-stimulated genes (**C**) *Viperin*, 2'-5'-oligoadenylate synthetase 1 (*OAS1*) and Myxovirus resistance protein 2 (*MX2*) as well as inflammasome genes (**D**) gasdermin D (*GSDMD*) and Caspase 1 (*Casp1*) are shown. Values are expressed as the mean of three independent experiments. Error bars represent standard errors of the mean. $*P < 0.05$, and $***P < 0.001$, by the Student *t* test.

Fig. 3. The anti-NOD2 drug GSK717 inhibits ZIKV replication. ZIKV-infected HFAs (MOI=0.05-5) were treated with DMSO or NOD2 blocking agent GSK717 after which viral titers were determined daily for up to 72-hours post-infection. ZIKV titers as relative fold (MOI=0.05) for 72 hours (**A**) and as PFU/mL at 48 hours post-infection (MOI=5) (**B**) are shown. Explants of human fetal brain (15-19 week old donors) were infected with the microcephalic ZIKV strain PRVABC-59 followed by GSK717 or DMSO treatment. Viral titers are shown as relative fold for

72 hours (**C**) and as PFU/mL at 48 hours post-infection (**D**). At 72 hours, the explant tissue was collected for viral RNA quantitation by qRT-PCR (**E**). Values are expressed as the mean of three independent experiments. Error bars represent standard errors of the mean. *$P < 0.05$, **$P < 0.01$, and ***$P < 0.001$, by the Student *t* test.

Fig. 4. The anti-NOD2 drug GSK717 blocks the spread of ZIKV infection. (**A**) Representative confocal imaging (20X) showing antiviral effect of GSK717 at 20 µM and 40 µM. A549 cells were infected with ZIKV (MOI=1) followed by treatment with DMSO or GSK717 at 20 or 40 µM for 48 hours before processing for indirect immunofluorescence. ZIKV-infected cells were identified using a mouse monoclonal antibody (4G2) to envelope protein and Alexa Fluor 488 donkey anti-mouse to detect the primary antibody. Nuclei were stained with DAPI. Images were acquired using a spinning disk confocal microscope equipped with Volocity 6.2.1 software. (**B**) Infected cells in 10 different fields from samples treated with GSK717 or DMSO were counted. Values are expressed as the mean of three independent experiments. Error bars represent standard errors of the mean. **$P < 0.01$, by the Student *t* test.

Fig. 5. The anti-NOD2 drug GSK717 inhibits DENV replication. A549 cells were infected with DENV-2 (MOI=0.05-5) and treated with GSK717 or DMSO for 48-hours after which cell culture media were harvested for plaque assay. Viral titers as relative fold using MOI of 0.05 or 5 (**A**) and as PFU/mL using MOI of 0.05 (**B**) or 5 (**C**) are shown. Cells were co-infected with DENV-2 and ZIKV (MOI=0.1) followed by GSK717 or DMSO treatment for 48 hours before collecting total cellular RNA for qRT-PCR. Viral RNA levels as relative fold (**D**) and as relative to mock (**E**) are presented. Values are expressed as the mean of three independent experiments. Error bars represent standard errors of the mean. *$P < 0.05$, **$P < 0.01$, and ***$P < 0.001$, by the Student *t* test.

Fig. 6. The anti-NOD2 drug GSK717 inhibits replication of MAYV and SARS-CoV-2 infection. A549 cells infected with low (0.05) and high (5) MOI of MAYV were treated with GSK717 or DMSO for 48 hours followed by collection of supernatants for plaque assay. Relative (**A**) and absolute (**B**) viral titers are shown with both MOI and with MOI of 0.05 respectively. Cells co-infected with MAYV and DENV-2 (MOI=0.1) were treated for 48 hours with GSK717 or DMSO before total cellular RNA was collected for qRT-PCR. Viral RNA data as relative fold (**C**) and as relative to mock (**D**) are shown. ACE2-SK-N-SH were infected with SARS-CoV-2 (MOI=0.05-5) and treated with GSK717 or DMSO for 48 hours after which culture supernatants were harvested for plaque assay. Viral titers as relative fold (**E**) and as PFU/mL (**F**) are shown using both MOI and the MOI of 0.05 respectively. Values are expressed as the mean of three independent experiments. Error bars represent standard errors of the mean. $*P < 0.05$, $**P < 0.01$, and $***P < 0.001$, by the Student *t* test.

Fig. 7. The anti-RIPK2 drug GSK583 has broad-spectrum antiviral activity. (**A**) A549 cells infected separately with three different arboviruses (MOI=0.1) were treated with the RIPK2 inhibitor GSK583 or DMSO alone for 24 hours followed by supernatant collection for plaque assay. Arbovirus titers as relative fold is presented. Cells were infected with ZIKV (**B**) or MAYV (**C)** at the MOI of 0.1 followed by the addition of GSK583 or DMSO immediately after infection (0 hours) or 24 hours post-infection. Viral titers, shown as relative fold, in supernatants were determined 24 hours after the treatment. ACE2-SK-N-SH cells infected with SARS-CoV-2 at low (0.05) and high (5) MOI were treated with GSK583 or DMSO for 24 hours followed by supernatant and total cellular RNA collection. Viral titers using both MOI as relative fold (**D**) and using MOI of 0.05 as PFU/mL (**E**) are shown. Relative viral RNA to mock level (**F**) with the MOI of 0.05 is

shown. Values are expressed as the mean of three independent experiments. Error bars represent standard errors of the mean. *$P < 0.05$, **$P < 0.01$, and ***$P < 0.001$, by the Student *t* test.

REFERENCES

1. Brechot C, Bryant J, Endtz H, Garry RF, Griffin DE, Lewin SR, Mercer N, Osterhaus A, Picot V, Vahlne A, Verjans GMGM, Weaver S. 2019. 2018 international meeting of the Global Virus Network. Antiviral Res 163:140-148.
2. De Clercq E, Li G. 2016. Approved Antiviral Drugs over the Past 50 Years. Clin Microbiol Rev 29:695-747.
3. Ianevski A, Andersen PI, Merits A, Bjørås M, Kainov D. 2019. Expanding the activity spectrum of antiviral agents. Drug Discov Today 24:1224-1228.
4. Ianevski A, Zusinaite E, Kuivanen S, Strand M, Lysvand H, Teppor M, Kakkola L, Paavilainen H, Laajala M, Kallio-Kokko H, Valkonen M, Kantele A, Telling K, Lutsar I, Letjuka P, Metelitsa N, Oksenych V, Bjørås M, Nordbø SA, Dumpis U, Vitkauskiene A, Öhrmalm C, Bondeson K, Bergqvist A, Aittokallio T, Cox RJ, Evander M, Hukkanen V, Marjomaki V, Julkunen I, Vapalahti O, Tenson T, Merits A, Kainov D. 2018. Novel activities of safe-in-human broad-spectrum antiviral agents. Antiviral Res 154:174-182.
5. Mukherjee T, Hovingh ES, Foerster EG, Abdel-Nour M, Philpott DJ, Girardin SE. 2019. NOD1 and NOD2 in inflammation, immunity and disease. Arch Biochem Biophys 670:69-81.
6. Cardinaud S, Urrutia A, Rouers A, Coulon PG, Kervevan J, Richetta C, Bet A, Maze EA, Larsen M, Iglesias MC, Appay V, Graff-Dubois S, Moris A. 2017. Triggering of TLR-3, -4, NOD2, and DC-SIGN reduces viral replication and increases T-cell activation capacity of HIV-infected human dendritic cells. Eur J Immunol 47:818-829.

7. Kapoor A, Forman M, Arav-Boger R. 2014. Activation of nucleotide oligomerization domain 2 (NOD2) by human cytomegalovirus initiates innate immune responses and restricts virus replication. PLoS One 9:e92704.

8. Vissers M, Remijn T, Oosting M, de Jong DJ, Diavatopoulos DA, Hermans PW, Ferwerda G. 2012. Respiratory syncytial virus infection augments NOD2 signaling in an IFN-β-dependent manner in human primary cells. Eur J Immunol 42:2727-35.

9. Tschöpe C, Müller I, Xia Y, Savvatis K, Pappritz K, Pinkert S, Lassner D, Heimesaat MM, Spillmann F, Miteva K, Bereswill S, Schultheiss HP, Fechner H, Pieske B, Kühl U, Van Linthout S. 2017. NOD2 (Nucleotide-Binding Oligomerization Domain 2) Is a Major Pathogenic Mediator of Coxsackievirus B3-Induced Myocarditis. Circ Heart Fail 10.

10. Limonta D, Jovel J, Kumar A, Lu J, Hou S, Airo AM, Lopez-Orozco J, Wong CP, Saito L, Branton W, Ka-Shu Wong G, Mason A, Power C, Hobman TC. 2019. Fibroblast growth factor 2 enhances Zika virus infection in human fetal brain. J Infect Dis 220:1377–1387.

11. Limonta D, Jovel J, Kumar A, Airo AM, Hou S, Saito L, Branton W, Ka-Shu Wong G, Mason A, Power C, Hobman TC. 2018. Human Fetal Astrocytes Infected with Zika Virus Exhibit Delayed Apoptosis and Resistance to Interferon: Implications for Persistence. Viruses 10.

12. de Sousa JR, Azevedo RDSD, Martins Filho AJ, de Araujo MTF, Cruz EDRM, Vasconcelos BCB, Cruz ACR, de Oliveira CS, Martins LC, Vasconcelos BHB, Casseb LMN, Chiang JO, Quaresma JAS, Vasconcelos PFDC. 2018. In situ inflammasome

activation results in severe damage to the central nervous system in fatal Zika virus microcephaly cases. Cytokine 111:255-264.

13. Tricarico PM, Caracciolo I, Crovella S, D'Agaro P. 2017. Zika virus induces inflammasome activation in the glial cell line U87-MG. Biochem Biophys Res Commun 492:597-602.

14. Rickard DJ, Sehon CA, Kasparcova V, Kallal LA, Zeng X, Montoute MN, Chordia T, Poore DD, Li H, Wu Z, Eidam PM, Haile PA, Yu J, Emery JG, Marquis RW, Gough PJ, Bertin J. 2013. Identification of benzimidazole diamides as selective inhibitors of the nucleotide-binding oligomerization domain 2 (NOD2) signaling pathway. PLoS One 8:e69619.

15. Limonta D, Branton W, Wong CP, Saito L, Power C, Hobman TC. 2020. Use of Primary Human Fetal Astrocytes and Tissue Explants as Ex Vivo Models to Study Zika Virus Infection of the Developing Brain. Methods Mol Biol 2142:251-259.

16. Mumtaz N, Jimmerson LC, Bushman LR, Kiser JJ, Aron G, Reusken CBEM, Koopmans MPG, van Kampen JJA. 2017. Cell-line dependent antiviral activity of sofosbuvir against Zika virus. Antiviral Res 146:161-163.

17. Katzelnick LC, Coloma J, Harris E. 2017. Dengue: knowledge gaps, unmet needs, and research priorities. Lancet Infect Dis 17:e88-e100.

18. Kinney RM, Butrapet S, Chang GJ, Tsuchiya KR, Roehrig JT, Bhamarapravati N, Gubler DJ. 1997. Construction of infectious cDNA clones for dengue 2 virus: strain 16681 and its attenuated vaccine derivative, strain PDK-53. Virology 230:300-8.

19. Silva MMO, Tauro LB, Kikuti M, Anjos RO, Santos VC, Gonçalves TSF, Paploski IAD, Moreira PSS, Nascimento LCJ, Campos GS, Ko AI, Weaver SC, Reis MG, Kitron U,

Ribeiro GS. 2019. Concomitant Transmission of Dengue, Chikungunya, and Zika Viruses in Brazil: Clinical and Epidemiological Findings From Surveillance for Acute Febrile Illness. Clin Infect Dis 69:1353-1359.

20. Carrillo-Hernández MY, Ruiz-Saenz J, Villamizar LJ, Gómez-Rangel SY, Martínez-Gutierrez M. 2018. Co-circulation and simultaneous co-infection of dengue, chikungunya, and zika viruses in patients with febrile syndrome at the Colombian-Venezuelan border. BMC Infect Dis 18:61.

21. Chia PY, Yew HS, Ho H, Chow A, Sadarangani SP, Chan M, Kam YW, Chong CY, Thoon KC, Yung CF, Li JH, Lye DC, De PP, Ng LFP, Yeo TW, Leo YS. 2017. Clinical features of patients with Zika and dengue virus co-infection in Singapore. J Infect 74:611-615.

22. Keestra-Gounder AM, Tsolis RM. 2017. NOD1 and NOD2: Beyond Peptidoglycan Sensing. Trends Immunol 38:758-767.

23. de Souza Costa MC, Siqueira Maia LM, Costa de Souza V, Gonzaga AM, Correa de Azevedo V, Ramos Martins L, Chavez Pavoni JH, Gomes Naveca F, Dezengrini Slhessarenko R. 2019. Arbovirus investigation in patients from Mato Grosso during Zika and Chikungunya virus introdution in Brazil, 2015-2016. Acta Trop 190:395-402.

24. Ratajczak MZ, Bujko K, Ciechanowicz A, Sielatycka K, Cymer M, Marlicz W, Kucia M. 2020. SARS-CoV-2 Entry Receptor ACE2 Is Expressed on Very Small CD45. Stem Cell Rev Rep.

25. Hoel H, Heggelund L, Reikvam DH, Stiksrud B, Ueland T, Michelsen AE, Otterdal K, Muller KE, Lind A, Muller F, Dudman S, Aukrust P, Dyrhol-Riise AM, Holter JC,

Trøseid M. 2020. Elevated markers of gut leakage and inflammasome activation in COVID-19 patients with cardiac involvement. J Intern Med.

26. Toldo S, Bussani R, Nuzzi V, Bonaventura A, Mauro AG, Cannatà A, Pillappa R, Sinagra G, Nana-Sinkam P, Sime P, Abbate A. 2020. Inflammasome formation in the lungs of patients with fatal COVID-19. Inflamm Res.

27. Humphries F, Yang S, Wang B, Moynagh PN. 2015. RIP kinases: key decision makers in cell death and innate immunity. Cell Death Differ 22:225-36.

28. Haile PA, Votta BJ, Marquis RW, Bury MJ, Mehlmann JF, Singhaus R, Charnley AK, Lakdawala AS, Convery MA, Lipshutz DB, Desai BM, Swift B, Capriotti CA, Berger SB, Mahajan MK, Reilly MA, Rivera EJ, Sun HH, Nagilla R, Beal AM, Finger JN, Cook MN, King BW, Ouellette MT, Totoritis RD, Pierdomenico M, Negroni A, Stronati L, Cucchiara S, Ziółkowski B, Vossenkämper A, MacDonald TT, Gough PJ, Bertin J, Casillas LN. 2016. The Identification and Pharmacological Characterization of 6-(tert-Butylsulfonyl)-N-(5-fluoro-1H-indazol-3-yl)quinolin-4-amine (GSK583), a Highly Potent and Selective Inhibitor of RIP2 Kinase. J Med Chem 59:4867-80.

29. Acosta-Ampudia Y, Monsalve DM, Rodríguez Y, Pacheco Y, Anaya JM, Ramírez-Santana C. 2018. Mayaro: an emerging viral threat? Emerg Microbes Infect 7:163.

30. Pierson TC, Diamond MS. 2018. The emergence of Zika virus and its new clinical syndromes. Nature 560:573-581.

31. Chen P, Nirula A, Heller B, Gottlieb RL, Boscia J, Morris J, Huhn G, Cardona J, Mocherla B, Stosor V, Shawa I, Adams AC, Van Naarden J, Custer KL, Shen L, Durante M, Oakley G, Schade AE, Sabo J, Patel DR, Klekotka P, Skovronsky DM, Investigators

B-. 2020. SARS-CoV-2 Neutralizing Antibody LY-CoV555 in Outpatients with Covid-19. N Engl J Med.

32. Stone JH, Frigault MJ, Serling-Boyd NJ, Fernandes AD, Harvey L, Foulkes AS, Horick NK, Healy BC, Shah R, Bensaci AM, Woolley AE, Nikiforow S, Lin N, Sagar M, Schrager H, Huckins DS, Axelrod M, Pincus MD, Fleisher J, Sacks CA, Dougan M, North CM, Halvorsen YD, Thurber TK, Dagher Z, Scherer A, Wallwork RS, Kim AY, Schoenfeld S, Sen P, Neilan TG, Perugino CA, Unizony SH, Collier DS, Matza MA, Yinh JM, Bowman KA, Meyerowitz E, Zafar A, Drobni ZD, Bolster MB, Kohler M, D'Silva KM, Dau J, Lockwood MM, Cubbison C, Weber BN, Mansour MK, Investigators BBTT. 2020. Efficacy of Tocilizumab in Patients Hospitalized with Covid-19. N Engl J Med.

33. Glasgow A, Glasgow J, Limonta D, Solomon P, Lui I, Zhang Y, Nix MA, Rettko NJ, Zha S, Yamin R, Kao K, Rosenberg OS, Ravetch JV, Wiita AP, Leung KK, Lim SA, Zhou XX, Hobman TC, Kortemme T, Wells JA. 2020. Engineered ACE2 receptor traps potently neutralize SARS-CoV-2. Proc Natl Acad Sci U S A.

34. Goldman JD, Lye DCB, Hui DS, Marks KM, Bruno R, Montejano R, Spinner CD, Galli M, Ahn MY, Nahass RG, Chen YS, SenGupta D, Hyland RH, Osinusi AO, Cao H, Blair C, Wei X, Gaggar A, Brainard DM, Towner WJ, Muñoz J, Mullane KM, Marty FM, Tashima KT, Diaz G, Subramanian A, Investigators G-U--. 2020. Remdesivir for 5 or 10 Days in Patients with Severe Covid-19. N Engl J Med.

35. Beigel JH, Tomashek KM, Dodd LE, Mehta AK, Zingman BS, Kalil AC, Hohmann E, Chu HY, Luetkemeyer A, Kline S, Lopez de Castilla D, Finberg RW, Dierberg K, Tapson V, Hsieh L, Patterson TF, Paredes R, Sweeney DA, Short WR, Touloumi G, Lye

DC, Ohmagari N, Oh MD, Ruiz-Palacios GM, Benfield T, Fätkenheuer G, Kortepeter MG, Atmar RL, Creech CB, Lundgren J, Babiker AG, Pett S, Neaton JD, Burgess TH, Bonnett T, Green M, Makowski M, Osinusi A, Nayak S, Lane HC, Members A-SG. 2020. Remdesivir for the Treatment of Covid-19 - Final Report. N Engl J Med.

36. WHO. 2020 Draft landscape of COVID-19 candidate vaccines. Accessed October 20, 2020

37. Rubin EJ, Baden LR, Piot P, Morrissey S. 2020. Audio Interview: New SARS-CoV-2 Vaccine Results, with Peter Piot. N Engl J Med 383:e57.

38. Hodgson SH, Mansatta K, Mallett G, Harris V, Emary KRW, Pollard AJ. 2020. What defines an efficacious COVID-19 vaccine? A review of the challenges assessing the clinical efficacy of vaccines against SARS-CoV-2. Lancet Infect Dis.

39. Tigno-Aranjuez JT, Asara JM, Abbott DW. 2010. Inhibition of RIP2's tyrosine kinase activity limits NOD2-driven cytokine responses. Genes Dev 24:2666-77.

40. Duran A, Valero N, Mosquera J, Fuenmayor E, Alvarez-Mon M. 2017. Gefitinib and pyrrolidine dithiocarbamate decrease viral replication and cytokine production in dengue virus infected human monocyte cultures. Life Sci 191:180-185.

41. Wiersinga WJ, Rhodes A, Cheng AC, Peacock SJ, Prescott HC. 2020. Pathophysiology, Transmission, Diagnosis, and Treatment of Coronavirus Disease 2019 (COVID-19): A Review. JAMA.

42. Gutjahr A, Papagno L, Vernejoul F, Lioux T, Jospin F, Chanut B, Perouzel E, Rochereau N, Appay V, Verrier B, Paul S. 2020. New chimeric TLR7/NOD2 agonist is a potent adjuvant to induce mucosal immune responses. EBioMedicine 58:102922.

43. Shafique M, Wilschut J, de Haan A. 2012. Induction of mucosal and systemic immunity against respiratory syncytial virus by inactivated virus supplemented with TLR9 and NOD2 ligands. Vaccine 30:597-606.

FIG 1

A

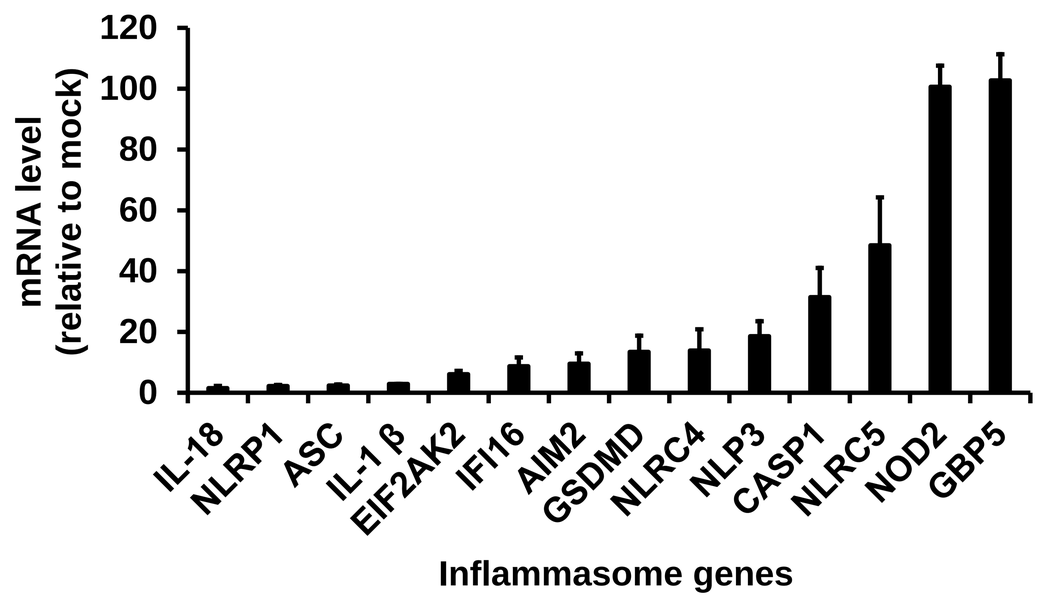
mRNA level
(relative to mock)
120
100
80
60
40
20
0
IL-18
NLRP1
ASC
IL-1 β
EIF2AK2
IFI16
AIM2
GSDMD
NLRC4
NLP3
CASP1
NLRC5
NOD2
GBP5
Inflammasome genes

B

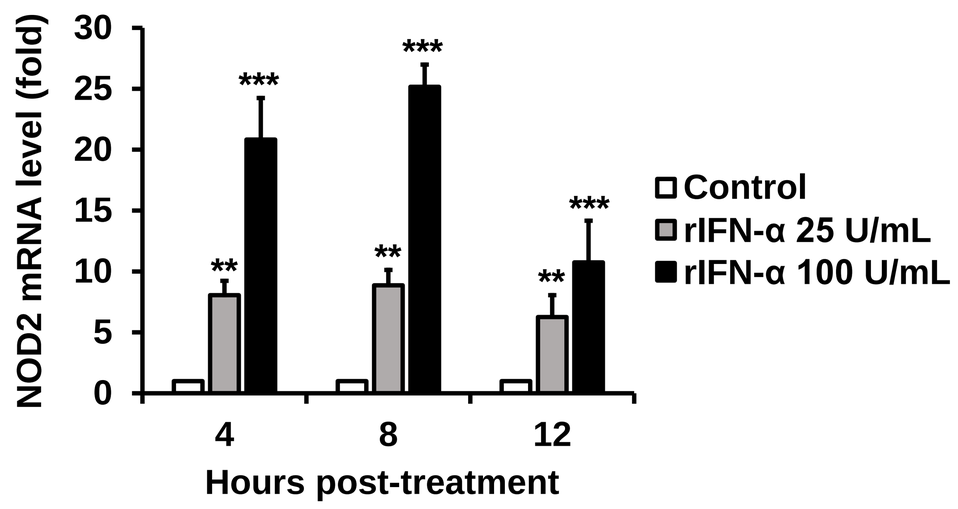
NOD2 mRNA level (fold)
30
25
20
15
10
5
0
***
**
***
**
***
**
4
8
12
Hours post-treatment
Control
rIFN-α 25 U/mL
rIFN-α 100 U/mL

C

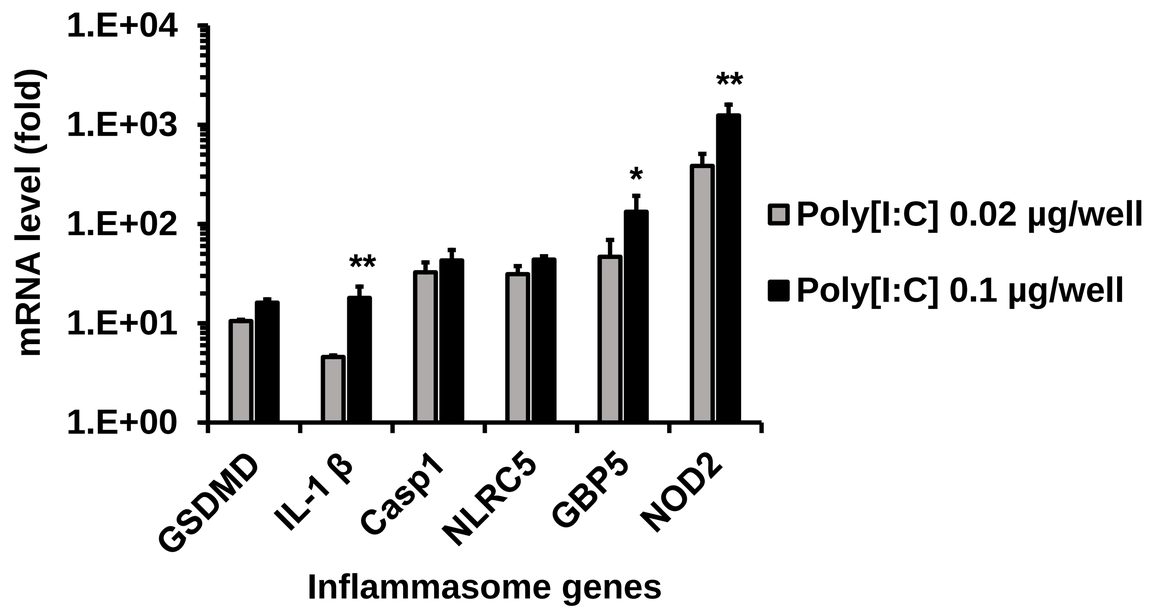
mRNA level (fold)
1.E+04
1.E+03
1.E+02
1.E+01
1.E+00
**
*
**
GSDMD
IL-1 β
Casp1
NLRC5
GBP5
NOD2
Inflammasome genes
Poly[I:C] 0.02 μg/well
Poly[I:C] 0.1 μg/well

FIG 2

A

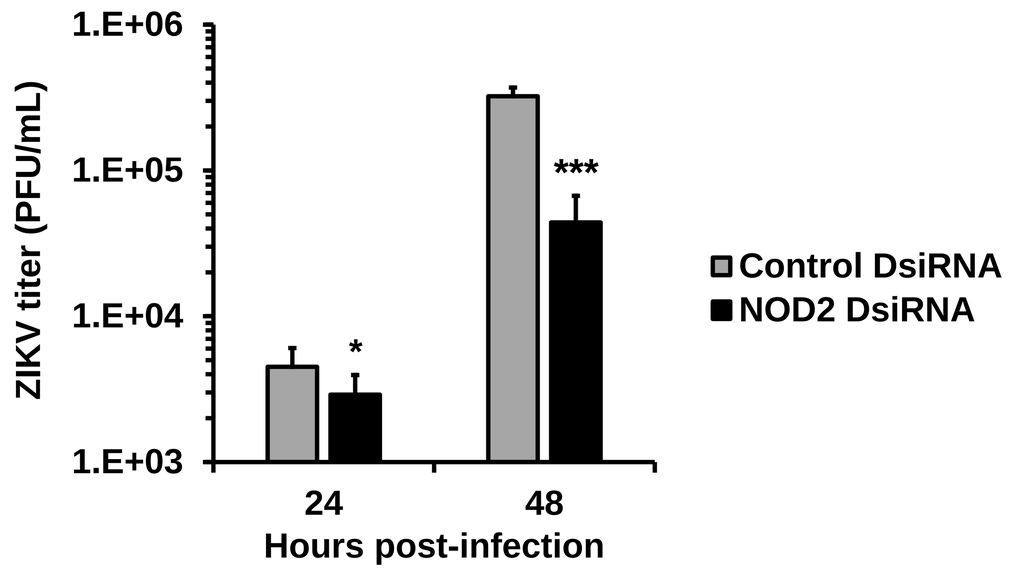
1.E+06
1.E+05
1.E+04
1.E+03
ZIKV titer (PFU/mL)
*
***
24
48
Hours post-infection
Control DsiRNA
NOD2 DsiRNA

B

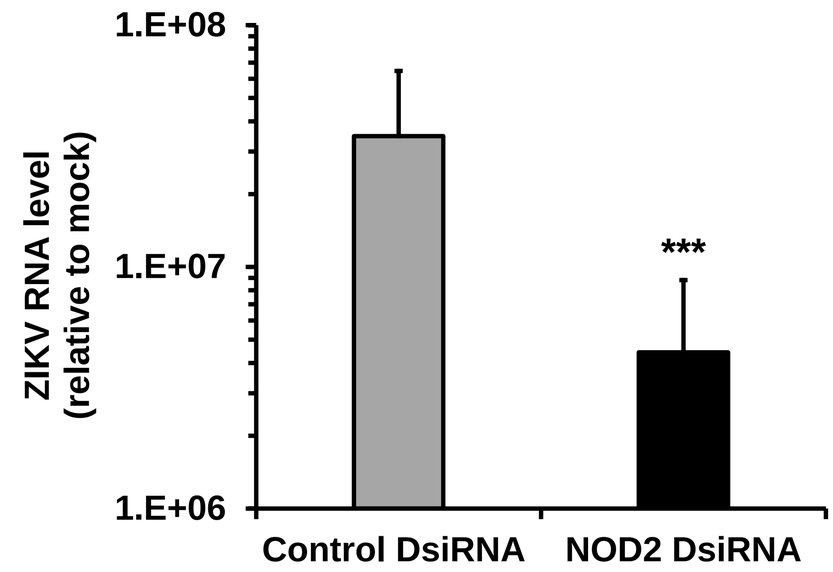
1.E+08
1.E+07
1.E+06
ZIKV RNA level
(relative to mock)
***
Control DsiRNA
NOD2 DsiRNA

C

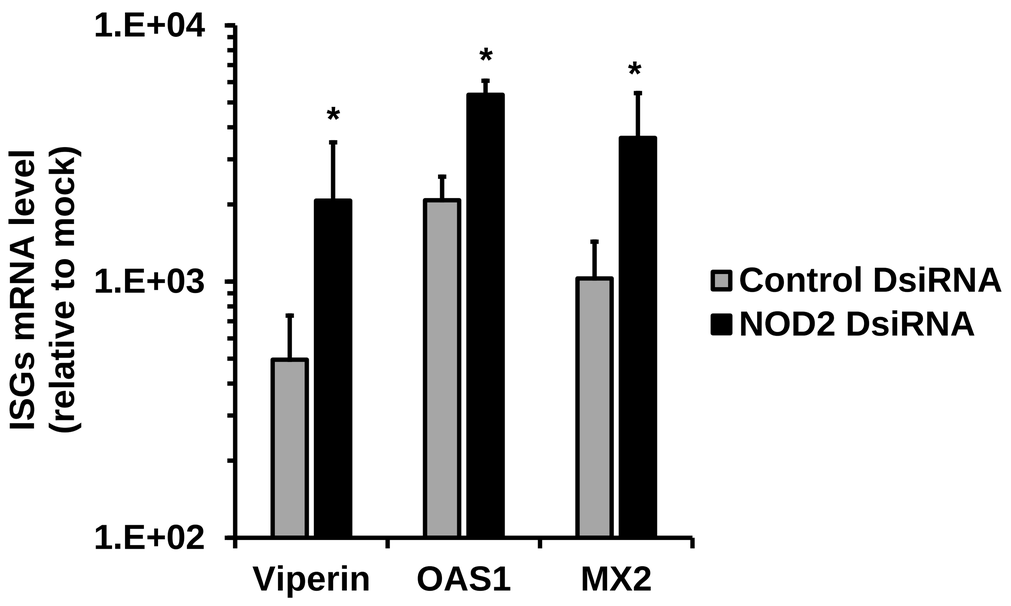
1.E+04
1.E+03
1.E+02
ISGs mRNA level
(relative to mock)
*
*
*
Viperin
OAS1
MX2
Control DsiRNA
NOD2 DsiRNA

D

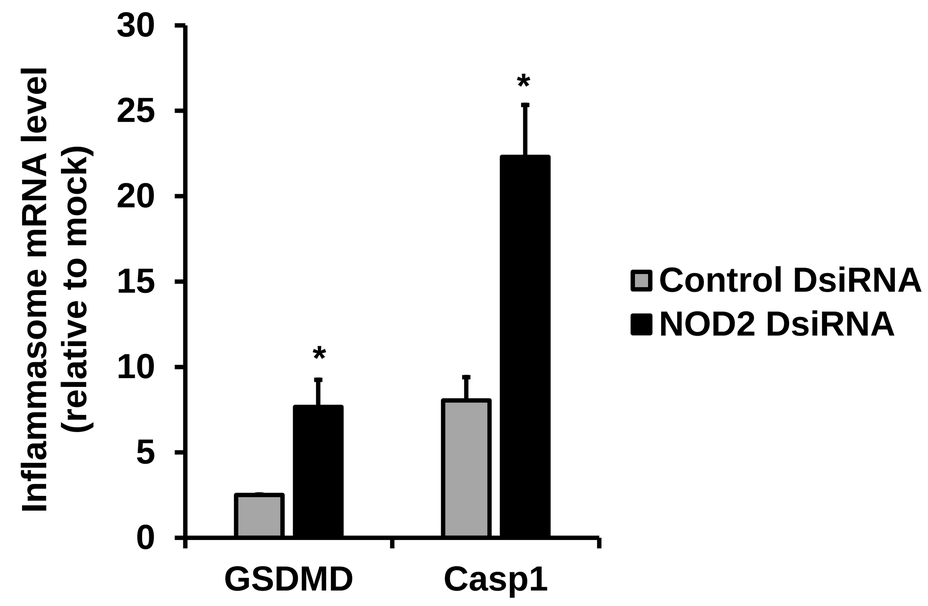
30
25
20
15
10
5
0
Inflammasome mRNA level
(relative to mock)
*
*
GSDMD
Casp1
Control DsiRNA
NOD2 DsiRNA

FIG 3

A

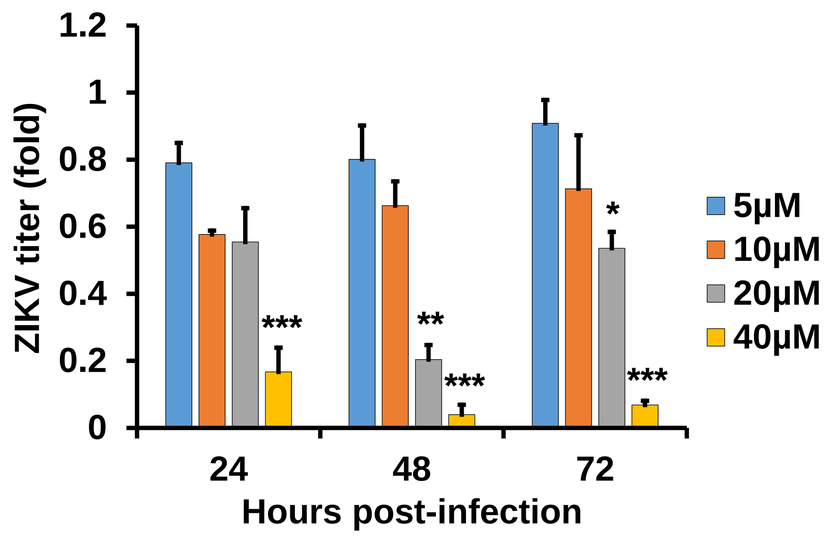
1.2
1
0.8
0.6
0.4
0.2
0
ZIKV titer (fold)
***
**
***
*
***
24
48
72
Hours post-infection
5μM
10μM
20μM
40μM

B

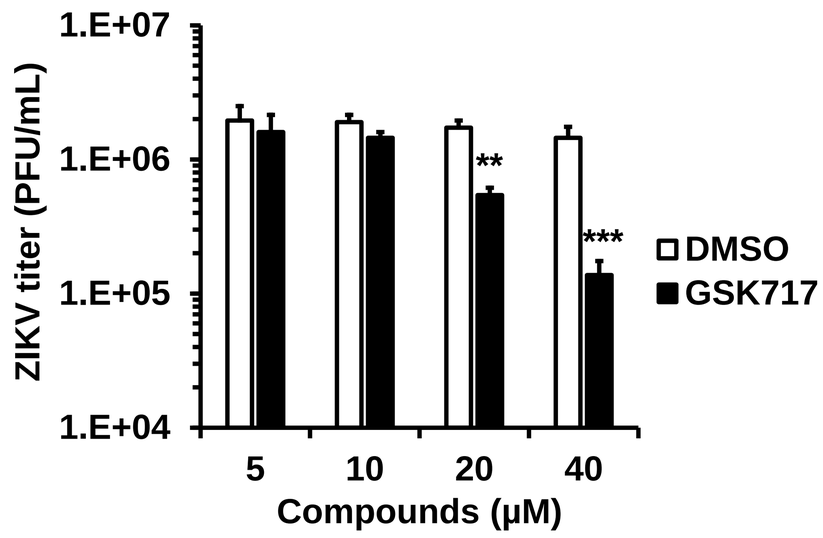
1.E+07
1.E+06
1.E+05
1.E+04
ZIKV titer (PFU/mL)
**
***
5
10
20
40
Compounds (μM)
DMSO
GSK717

C

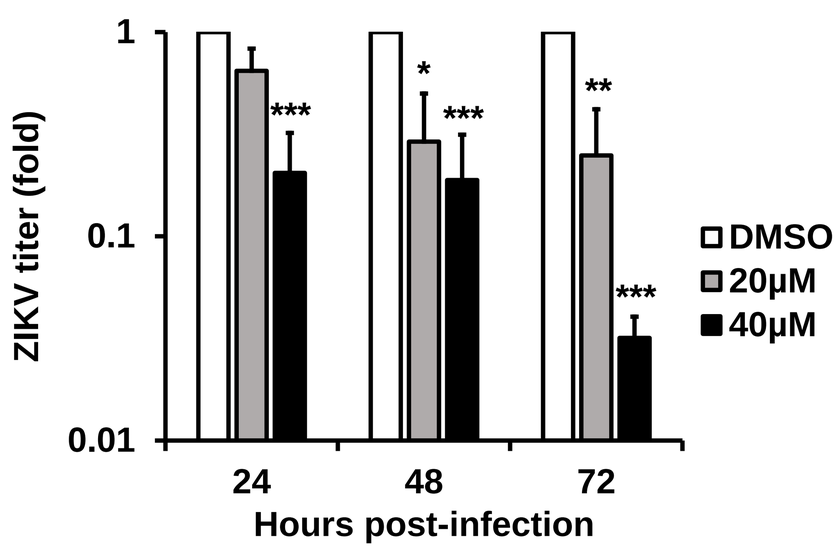
1
0.1
0.01
ZIKV titer (fold)
***
*
***
**
***
24
48
72
Hours post-infection
DMSO
20μM
40μM

D

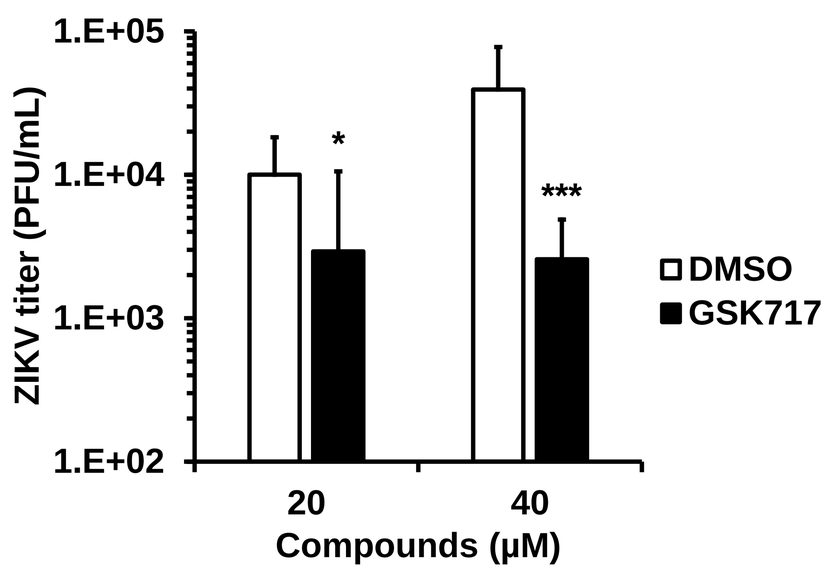
1.E+05
1.E+04
1.E+03
1.E+02
ZIKV titer (PFU/mL)
*
***
20
40
Compounds (μM)
DMSO
GSK717

E

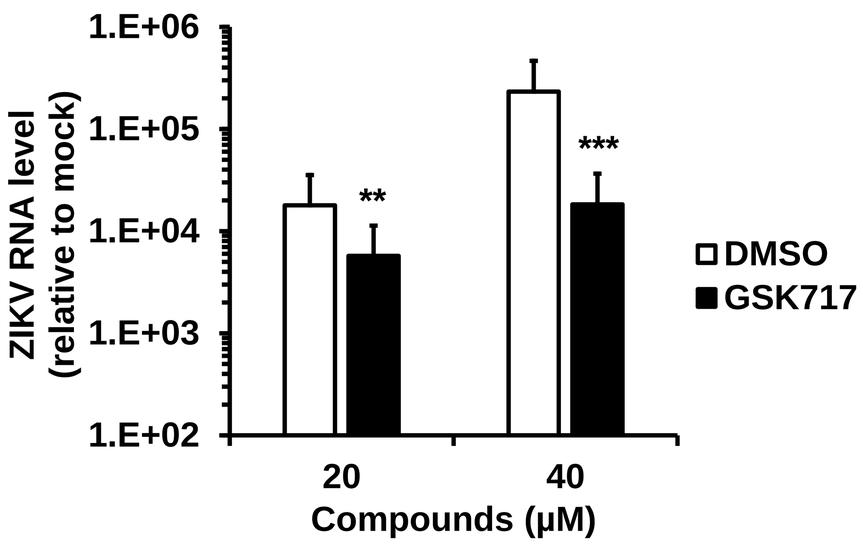
1.E+06
1.E+05
1.E+04
1.E+03
1.E+02
ZIKV RNA level
(relative to mock)
**
***
20
40
Compounds (μM)
DMSO
GSK717

FIG 4

A

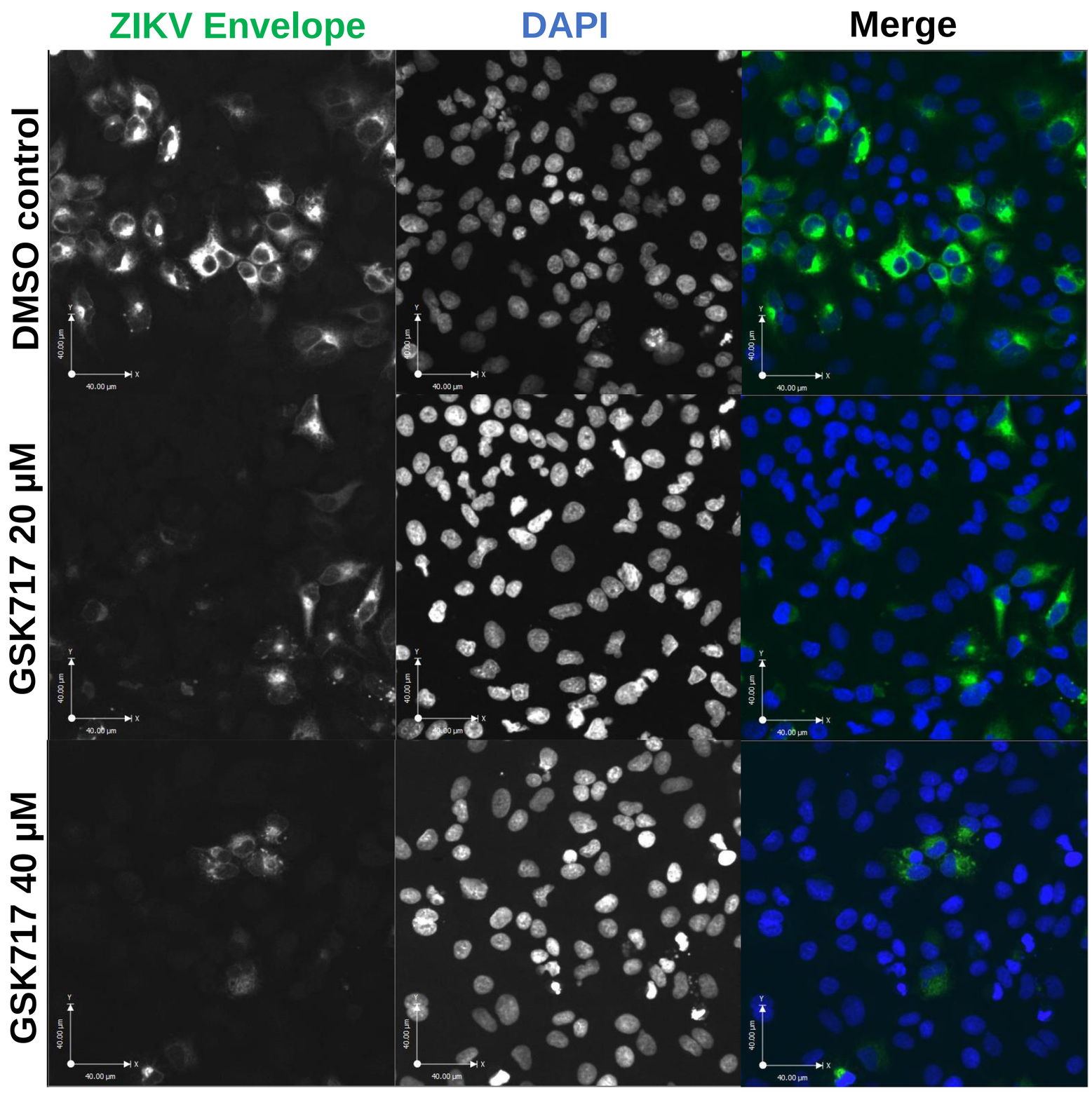
ZIKV Envelope
DAPI
Merge
DMSO control
GSK717 20 μM
GSK717 40 μM

B

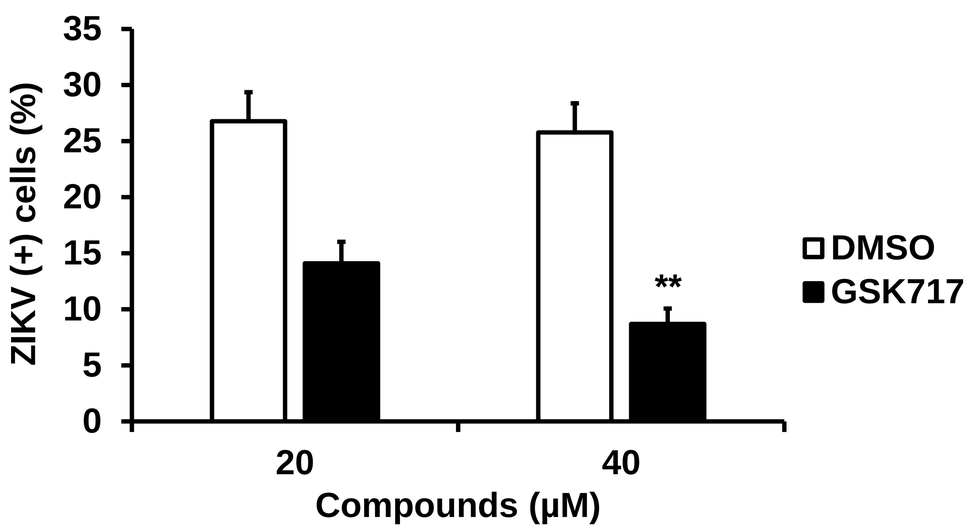
ZIKV (+) cells (%)
35
30
25
20
15
10
5
0
**
20
40
Compounds (μM)
DMSO
GSK717

FIG 5

A

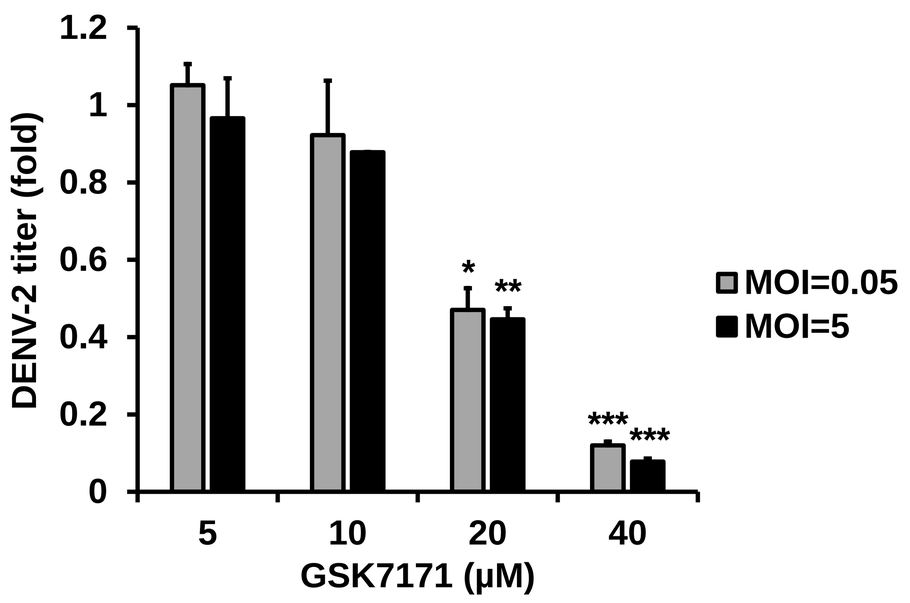
1.2
1
0.8
0.6
0.4
0.2
0
DENV-2 titer (fold)
*
**
***
***
MOI=0.05
MOI=5
5
10
20
40
GSK7171 (μM)

B

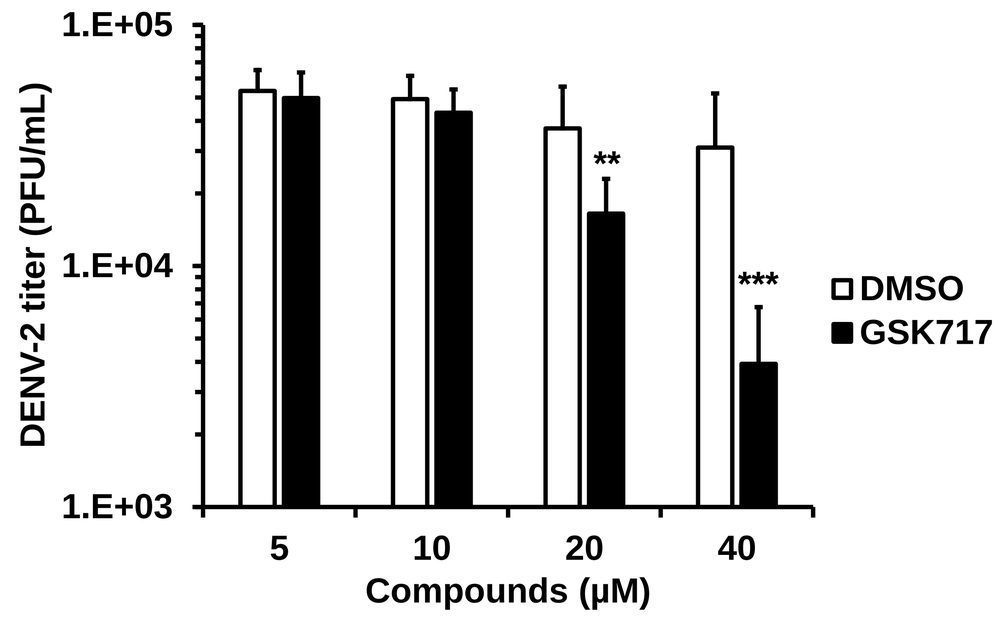
1.E+05
1.E+04
1.E+03
DENV-2 titer (PFU/mL)
**
***
DMSO
GSK717
5
10
20
40
Compounds (μM)

C

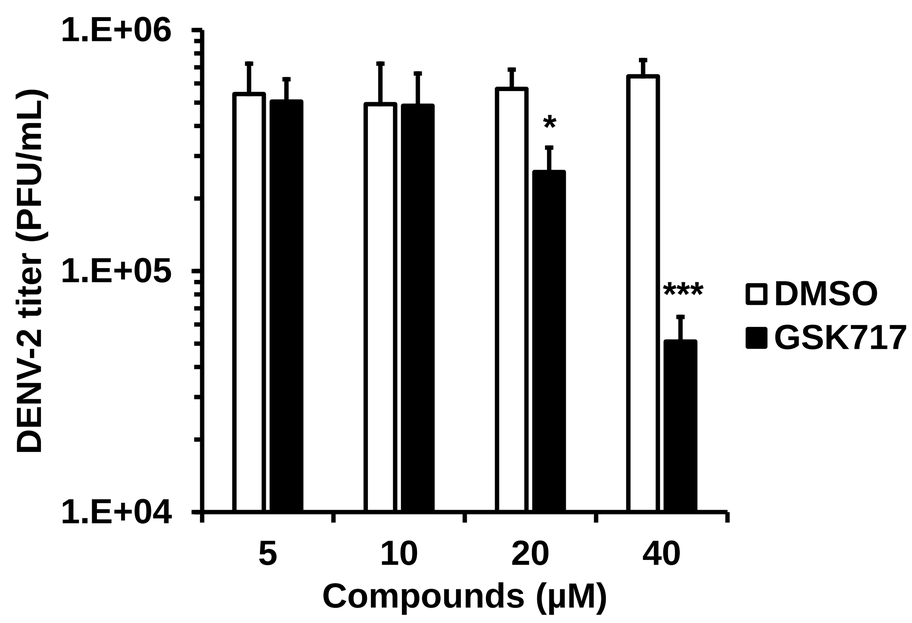
1.E+06
1.E+05
1.E+04
DENV-2 titer (PFU/mL)
*
***
DMSO
GSK717
5
10
20
40
Compounds (μM)

D

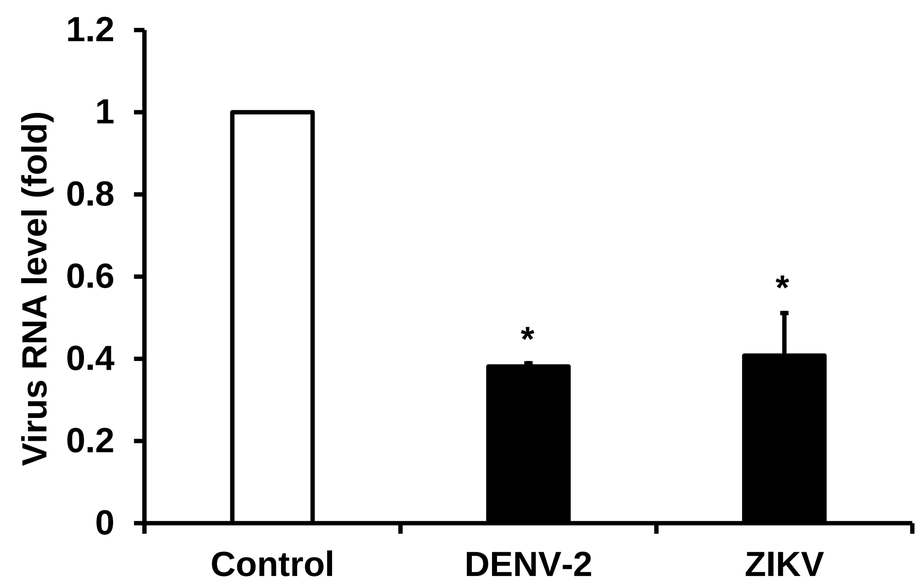
1.2
1
0.8
0.6
0.4
0.2
0
Virus RNA level (fold)
*
*
Control
DENV-2
ZIKV

E

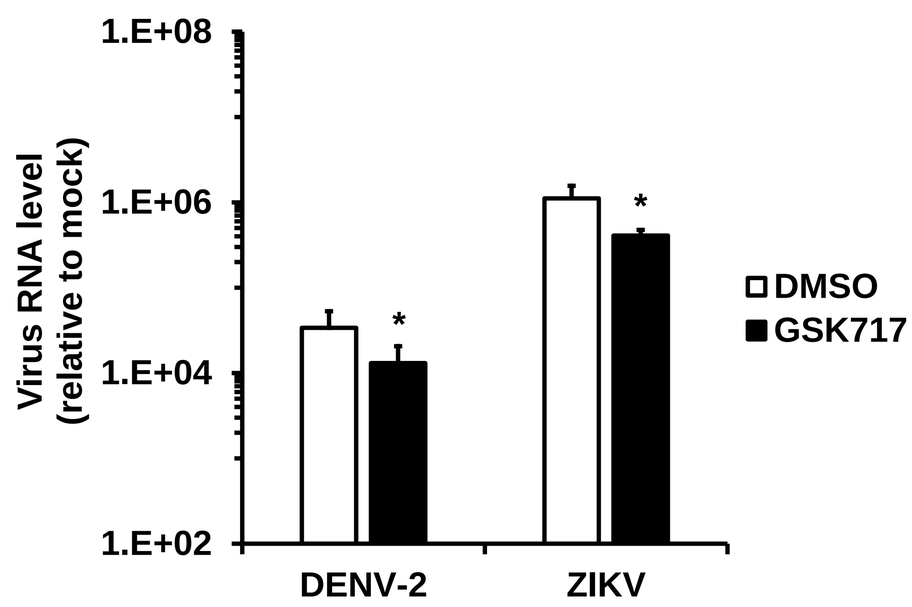
1.E+08
1.E+06
1.E+04
1.E+02
Virus RNA level
(relative to mock)
*
*
DMSO
GSK717
DENV-2
ZIKV

FIG 6

A

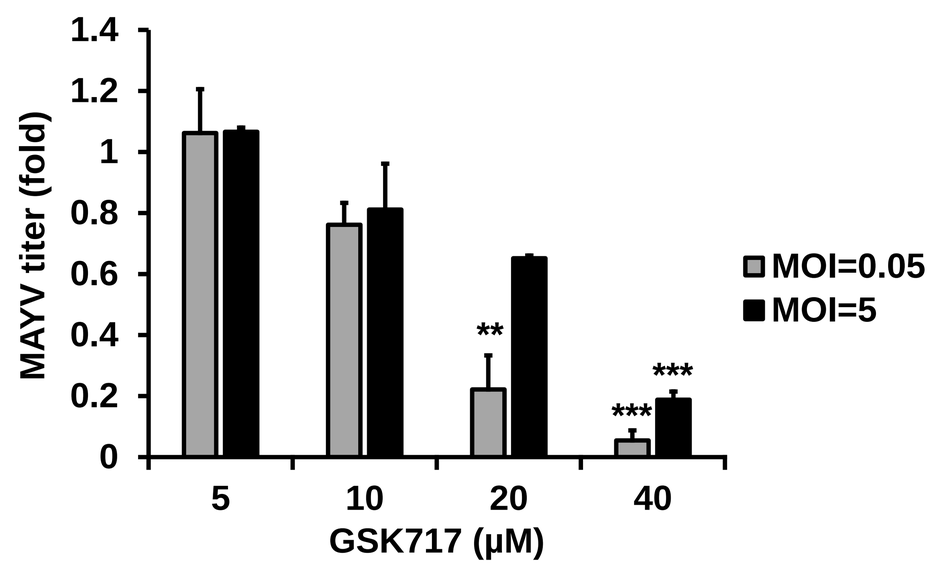
MAYV titer (fold)
1.4
1.2
1
0.8
0.6
0.4
0.2
0
**
***
***
5
10
20
40
GSK717 (μM)
MOI=0.05
MOI=5

B

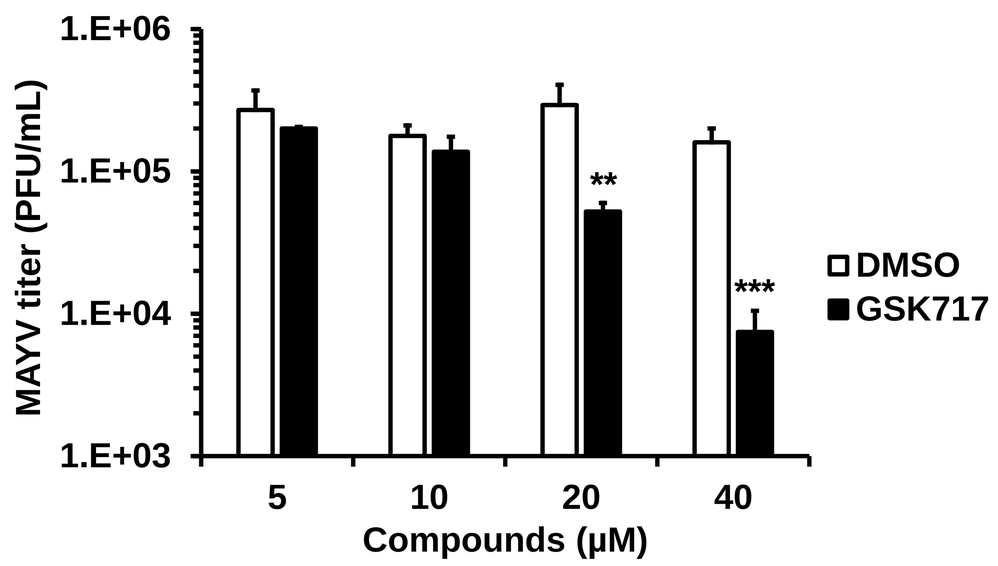
MAYV titer (PFU/mL)
1.E+06
1.E+05
1.E+04
1.E+03
**
***
5
10
20
40
Compounds (μM)
DMSO
GSK717

C

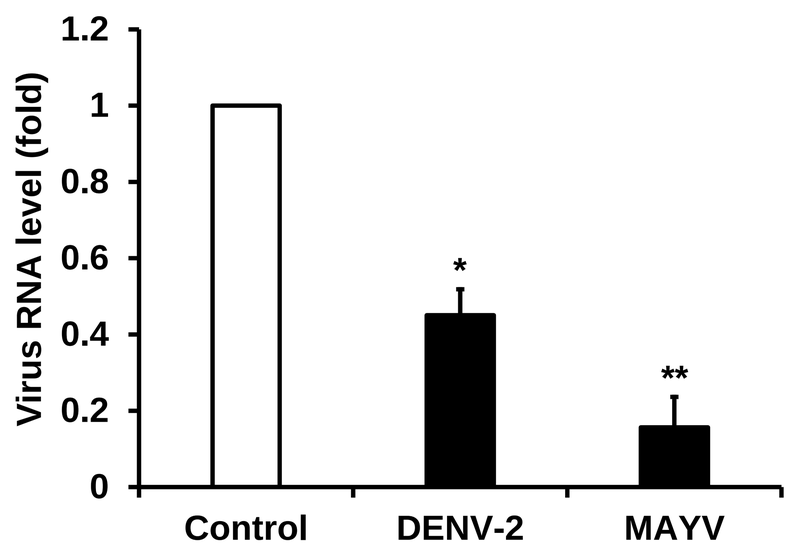
Virus RNA level (fold)
1.2
1
0.8
0.6
0.4
0.2
0
*
**
Control
DENV-2
MAYV

D

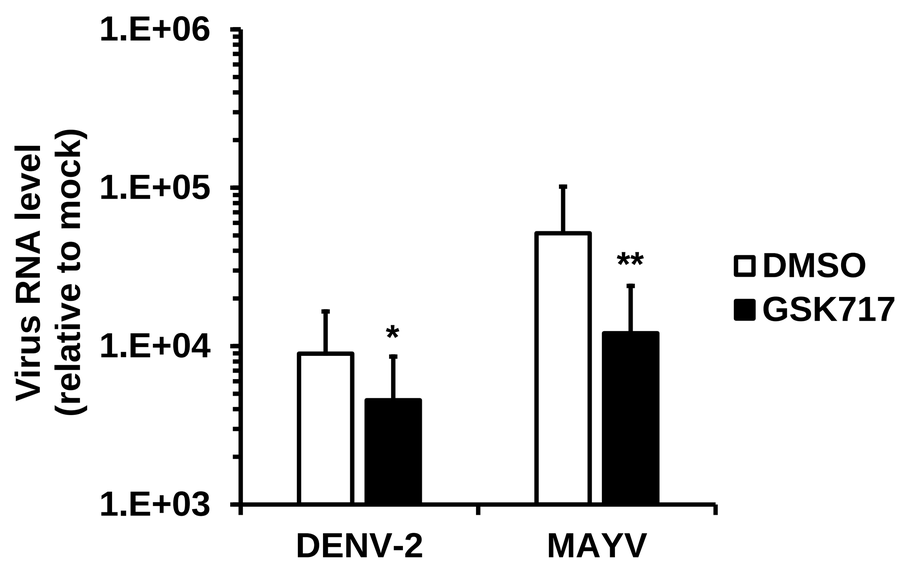
Virus RNA level (relative to mock)
1.E+06
1.E+05
1.E+04
1.E+03
*
**
DENV-2
MAYV
DMSO
GSK717

E

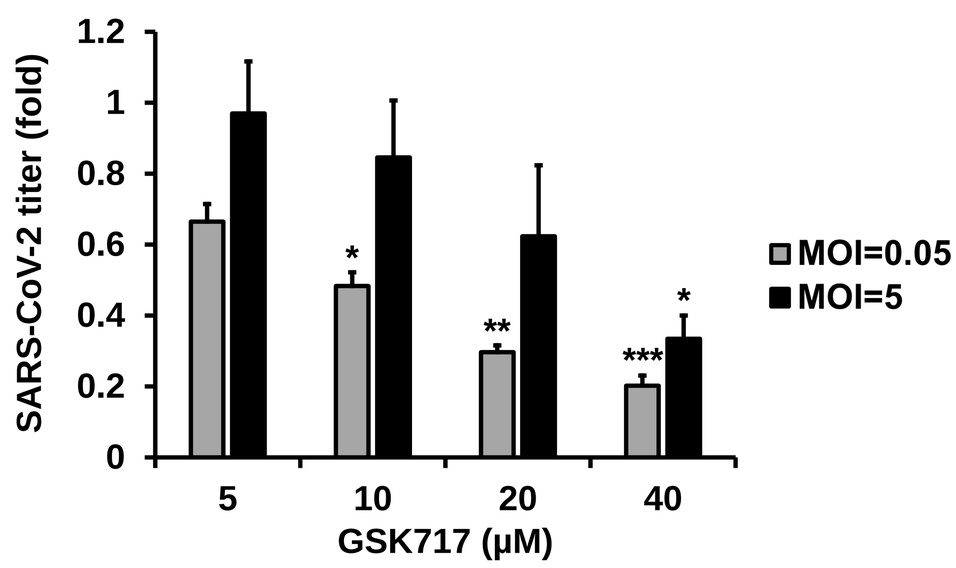
SARS-CoV-2 titer (fold)
1.2
1
0.8
0.6
0.4
0.2
0
*
**
***
*
5
10
20
40
GSK717 (μM)
MOI=0.05
MOI=5

F

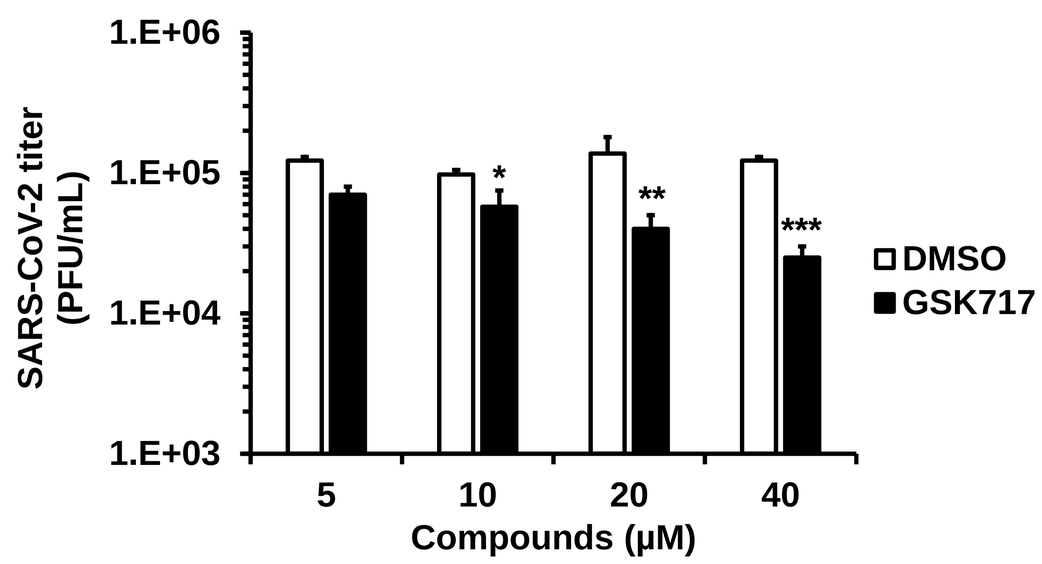
SARS-CoV-2 titer (PFU/mL)
1.E+06
1.E+05
1.E+04
1.E+03
*
**
***
5
10
20
40
Compounds (μM)
DMSO
GSK717

FIG 7

A

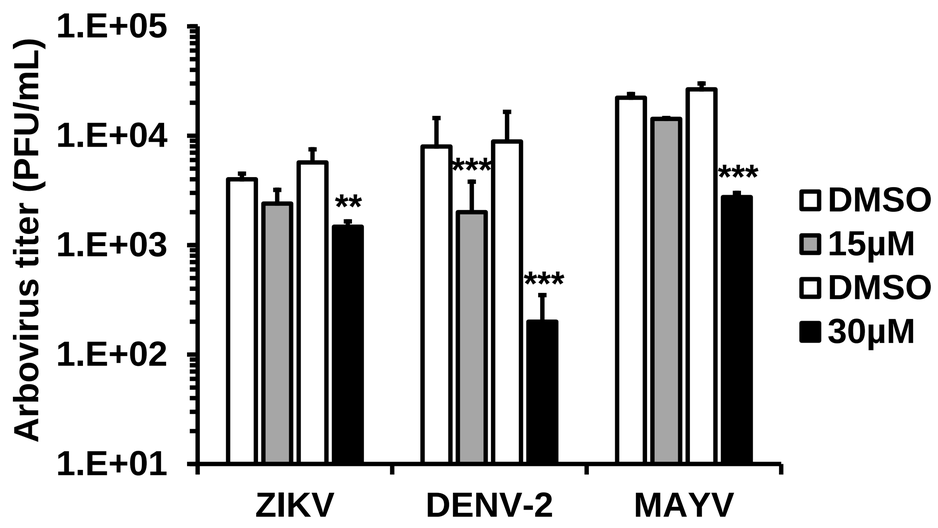
Arbovirus titer (PFU/mL)
1.E+05
1.E+04
1.E+03
1.E+02
1.E+01
**
***
***
***
ZIKV
DENV-2
MAYV
DMSO
15μM
DMSO
30μM

B

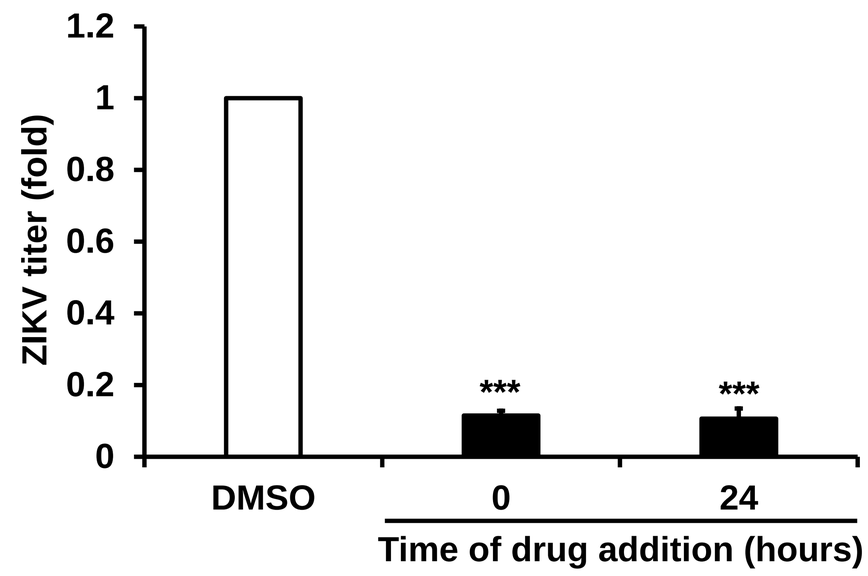
ZIKV titer (fold)
1.2
1
0.8
0.6
0.4
0.2
0
***
***
DMSO
0
24
Time of drug addition (hours)

C

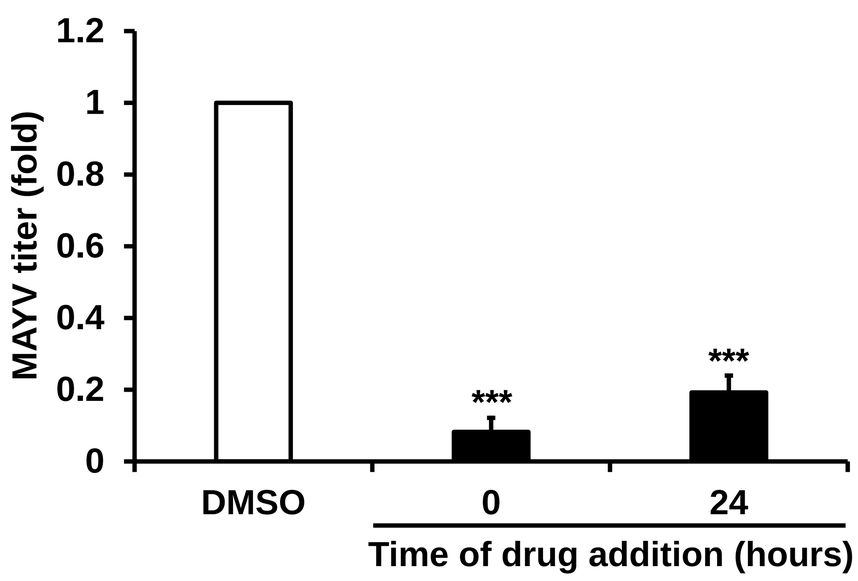
MAYV titer (fold)
1.2
1
0.8
0.6
0.4
0.2
0
***
***
DMSO
0
24
Time of drug addition (hours)

D

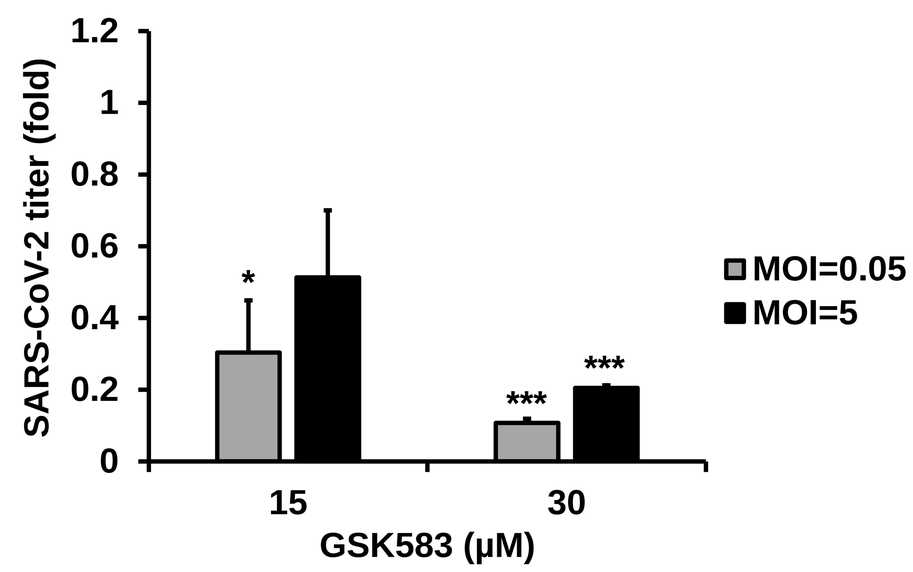
SARS-CoV-2 titer (fold)
1.2
1
0.8
0.6
0.4
0.2
0
*
***
***
MOI=0.05
MOI=5
15
30
GSK583 (μM)

E

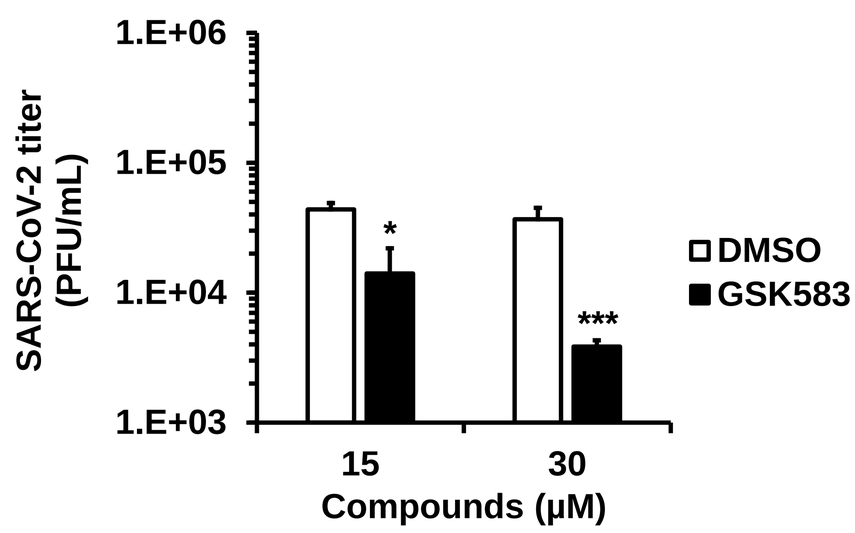
SARS-CoV-2 titer (PFU/mL)
1.E+06
1.E+05
1.E+04
1.E+03
*
***
DMSO
GSK583
15
30
Compounds (μM)

F

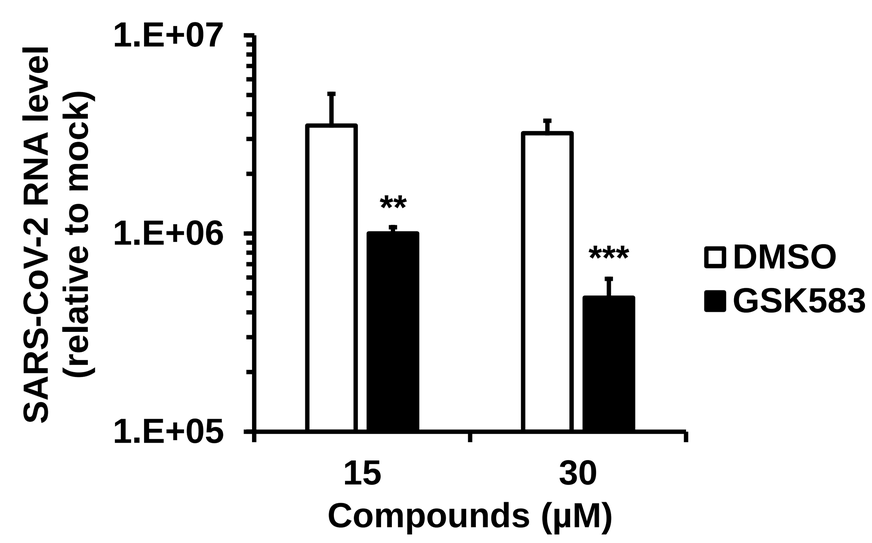
SARS-CoV-2 RNA level (relative to mock)
1.E+07
1.E+06
1.E+05
**
***
DMSO
GSK583
15
30
Compounds (μM)

SUPPLEMENTAL MATERIAL

Nodosome inhibition as a novel broad-spectrum antiviral strategy against arboviruses and SARS-CoV-2

Daniel Limonta, Lovely Dyna-Dagman, William Branton, Tadashi Makio, Richard W. Wozniak, Christopher Power, Tom C. Hobman

Cells and viruses. The prototype Zika virus (ZIKV) strain isolated in Puerto Rico (PRVABC-59) in 2015 (1) was kindly provided by the National Microbiology Laboratory of Canada (Winnipeg, Canada). Dengue virus-2 (DENV-2, 16681 strain) clone was provided by Dr. Bart Bartenschlager at the Heidelberg University Hospital (Heidelberg, Germany). Mayaro virus (MAYV, TRVL 15537) strain was obtained from ATCC. Arboviruses were propagated in *Aedes albopictus* C6/36 cells grown in MEM (Thermo Fisher Scientific) supplemented with 10% fetal bovine serum (Thermo Fisher Scientific), L-glutamine, Penicillin-Streptomycin and MEM non-essential amino acids at 32°C.

Arbovirus stocks were prepared after inoculating C6/36 cells using a multiplicity of infection (MOI) of 0.2 and then harvesting cell culture media between 24 to 96 hours post-infection. Virus-containing media were clarified by centrifugation at 3200 x g for 10 minutes. Human fetal astrocytes (HFAs) were prepared as previously described (2). Briefly, human fetal brain tissues were obtained from 15 to 19-week aborted fetuses. After isolation of astrocytes, cells were split, and all experiments were conducted with cells between the fifth and seventh passages. HFAs were grown in MEM supplemented with 10% fetal bovine serum, 15 mM HEPES (Thermo Fisher

Scientific) L-glutamine, MEM non-essential amino acids, sodium pyruvate, and 1g/mL glucose. Vero cells (ATCC, CCL-81) were maintained in DMEM supplemented with 10% fetal bovine serum, 15 mM HEPES, L-glutamine and Penicillin-Streptomycin.

Severe acute respiratory syndrome coronavirus 2 (SARS-CoV-2/CANADA/VIDO 01/2020) was kindly provided by Dr. Darryl Falzarano (Vaccine and Infectious Disease Organization-International Vaccine Centre, University of Saskatchewan, Canada). SARS-CoV-2 strain was propagated in Vero-E6 cells (ATCC) grown in DMEM supplemented with 10% fetal bovine serum, 15 mM HEPES, L-glutamine and Penicillin-Streptomycin.

A549, Huh7, and U251 (ATCC) and ACE2-hyperexpressing SK-N-SH cells were maintained in DMEM while HEL-18 human primary embryonic pulmonary fibroblasts (3) and Calu-3 (ATCC) were maintained in RPMI 1640 (Thermo Fisher Scientific) medium and MEM respectively supplemented with 10% fetal bovine serum, 15 mM HEPES, L-glutamine and Penicillin-Streptomycin.

Generation of ACE2-SK-N-SH cells. SK-N-SH cells stably expressing ACE2 were constructed using lentivirus transduction (4, 5). The coding region of the human ACE2 gene from the plasmid hACE2 (Addgene plasmid #1786) (6) was subcloned into the lentiviral vector pLenti-puro (Addgene plasmid #39481) (7) to generate pLenti-ACE2. Next, lentiviral pseudoparticles were harvested from the media of HEK293T cells (ATCC) transfected with viral packaging vectors (5) and pLenti-ACE2 using Lipofectamine 3000 (Invitrogen). SK-N-SH cells (ATCC) were transduced with the lentiviral pseudoparticles and stably transduced cells were selected using 10 μg/mL puromycin in DMEM containing 10% FBS. Expression of ACE2 protein was confirmed by western blotting using anti-ACE2 antibodies (R & D Systems).

Viral infections of cells. Cells were seeded in 96-wells plates (Greiner) at 1-2 x 10^4 cells per well. The next day, cells were rinsed once with PBS and viruses at an MOI of 0.05 to 5 were added to the wells. Cells were then incubated for 1 (SARS-CoV-2), 2 (arboviruses) or 3 (arboviral co-infections) hours at 37°C using fresh media supplemented with 3% fetal bovine serum. Next, the inoculum was removed, and the cells were washed twice with PBS. Complete culture medium was added to each well, and cells were incubated at 37°C and 5% CO_2. Mock-infected cells were incubated with the culture supernatant from uninfected cells.

Fetal brain explant cultures and infections. Human brain tissue from two 15-19-week aborted fetuses was obtained (after written consent) under protocol 1420 of the University of Alberta Human Research Ethics Board. After delivery to the laboratory in ice-cold PBS, the fresh tissue was placed in a 100 mM Petri dish and then dissected with sterile scalpel and forceps into approximately 5 mm x 5 cm x 1 mm blocks (2). The small tissue blocks were immediately immersed in 24-well plates containing the same media used to culture HFAs (see above).

Brain explant tissue was infected overnight with 10^6 PFU/mL of PRVABC-59 ZIKV strain. The next day, explants were washed once with PBS and then fresh media was added. The explant cultures were maintained in a humidified 37°C incubator containing 5% CO_2 for up to 5 days under different experimental treatments.

Tissue and cellular RNA purification, cDNA synthesis, and qRT-PCR. Total RNA was extracted from cultured cells or fetal brain tissue using NucleoSpin RNA (Macherey-Nagel GmbH & Co) kits. Samples were then treated with RNase-free DNase (Macherey-Nagel GmbH & Co) before a portion (0.5-1 µg total RNA) was subjected to reverse transcription using ImProm-II Reverse Transcriptase (Promega). Cellular transcripts and viral RNA were quantitated by qRT-

PCR using PerfeCTa SYBR Green SuperMix (Quanta BioSciences) in a CFX96 Touch Real-Time PCR Detection System instrument (Bio-Rad) under the following cycling conditions: 40 cycles of 94°C for 30 s, 55°C for 60 s, and 68°C for 20 s. Gene expression (fold change) was calculated using the $2^{(-\Delta\Delta CT)}$ method with human β-actin mRNA transcript as the internal control.

The following forward and reverse primer pairs were used for PCR:

Primer name	**Sequence**
β-actin	5'-GGATCAGCAAGCAGGAGTATG-3' 5'-GCATTTGCGGTGGACGAT-3'
NOD2 (nucleotide-binding oligomerization domain-containing protein 2)	5'-TCTCTGTGCGGACTCTACTC-3' 5'-ATCCGTGAACCTGAACTTG-3'
RSAD2 (radical SAM domain-containing 2 or viperin)	5'-CTTTTGCTGGGAAGCTCTTG-3' 5'-CAGCTGCTGCTTTCTCCTCT-3'
GSDMD (gasdermin D)	5'-GTGTGTCAACCTGTCTATCAAGG-3' 5'-CATGGCATCGTAGAAGTGGAAG-3'
Casp1 (caspase 1)	5'-TCACTGCTTCGGACATGACTACA-3' 5'-GGAACGTGCTGTCAGAGGTCTT-3'
GBP5 (guanylate binding protein 5)	5'-TCCTCGGATTATTGCTCGGC-3' 5'- CCTTTGCGCTTCAGCCTTTT-3'
NLRC5 (NOD-like receptor family CARD domain containing 5)	5'-TGGGAAGACACTCAGGCTAA-3' 5'-ATCATCGTCCTCACAGAGGTT-3'
IL-18 (Interleukin-18)	5'- GACTGTAGAGATAATGCAC-3'

	5’-CTTCGTTTTGAACAGTGAAC-3’
NLRP1 (NLR Family Pyrin Domain Containing 1)	5’-ACCATGGTAGTCCTGTTCAG-3’ 5’-GCGAGTTTCCACTTAGGTC-3’
ASC (apoptosis-associated speck like protein containing a caspase recruitment domain)	5’-GCACTTTATAGACCAGCACCG-3’ 5’-CTGAAGAGCTTCCGCATCTTG-3’
IL-1 β (Interleukin-1 β)	5’-AACCTCTTCGAGGCACAAGG-3’ 5’-GTCCTGGAAGGAGCACTTCAT-3’
EIF2AK2 (eukaryotic translation initiation factor 2-alpha kinase 2)	5’-ACCTCAGTGAAATCTGACTACC-3’ 5’-CAGATGATGATTCAGAAGCG -3’
IFI-16 (gamma-interferon-inducible protein 16)	5’- ACAAACCCGAGAAACAATGACC-3’ 5’- GCATCTGAGGAGTCCGAAGA-3’
NLRC4 (NOD-like receptor family CARD domain containing 4)	5’-CTGAGCAGCCTGTTGAAAC-3’ 5’-CATCCATCACTGCTCACAC-3’
NLRP3 (NLR family pyrin domain containing 3)	5’-CCAAGAATCCACAGTGTAACC-3’ 5’-CTTCACAGAACATCATGACCC-3’
OAS-1 (2'-5'-oligoadenylate synthetase 1)	5’- TTCTTAAAGCATGGGTAATTC-3’ 5’- GAAGGCAGCTCACGAAAC-3’
MX2 (Myxovirus resistance protein 2 or interferon-induced GTP-binding protein MX2)	5’-CAGCCACCACCAGGAAACA-3’ 5’-TTCTGCTCGTACTGGCTGTACAG-3’
ZIKV (8)	5’-CCTTGGATTCTTGAACGAGGA-3’ 5’-AGAGCTTCATTCTCCAGATCAA-3’

DENV (9)	5'-TTGAGTAAACTGTGCAGCCTGTAGCTC-3' 5'-GGGTCTCCTCTAACCTCTAGTCCT-3'
MAYV (10)	5'-AAGCTCTTCCTCTGCATTGC-3' 5'-TGCTGGAAACGCTCTCTGTA-3'
SARS-CoV-2 (11)	5'-CAATGGTTTAACAGGCACAGG-3' 5'-CTCAAGTGTCTGTGGATCACG-3'

Viral titer assay. Flaviviruses and alphaviruses were serially diluted (10-fold dilutions) and monolayers of Vero CCL-81 cells at 37 °C were infected for 2 hours. For the SARS-CoV-2 plaque assay, Vero-E6 cells were infected for 1 hour in a biosafety level 3 laboratory of the University of Alberta. The monolayers were overlaid with a mixture of MEM (Thermo Fisher Scientific) and 0.75-1.5% carboxymethylcellulose (Sigma-Aldrich) following infection. The cells were maintained at 37 °C for 2-7 days, depending on the virus (2 days for MAYV, 3 days for SARS-CoV-2, 4 days for ZIKV, and 7 days for DENV-2) for plaque development. Cells were fixed with 10% formaldehyde and stained with 1% crystal violet in 20% ethanol after which plaques were counted.

Cytotoxicity assays. The CellTiter-Glo Luminescent Cell Viability Assay (Promega) was used for quantitation of ATP in cultured cells. Cells lysates were assayed after mixing 100 µl of complete media with 100 µl of reconstituted CellTiter-Glo Reagent (buffer plus substrate) following the manufacturer's instructions. Samples were mixed by shaking the plates after which luminescence was recorded with a GloMax Explorer Model GM3510 (Promega) 10 min after adding the reagent.

Antiviral drug assays. Unless otherwise indicated, cells were cultured in 96-well plates (Greiner) and viral replication and titers were determined by qRT-PCR on total RNA extracted from cells

and plaque assay of cell supernatants respectively. Cells seeded into 96-well plates (Greiner) at 1-2 x 10^4 cells per well were infected the next day with ZIKV, DENV-2, MAYV or SARS-CoV-2 (MOI=0.05-5) followed by treatment with 5, 10, 20 and 40 µM of GSK717 (12) (Sigma-Aldrich) or an equal volume of DMSO. Viral replication and titers were determined 24 to 72-hours post-infection.

HFAs (5 x 10^4 cells per well) were grown in 24-well plates (Greiner) and after ZIKV infection (MOI=0.05-5), GSK717 (5-40 µM) was added to carry out a 3-day kinetics of viral titers. ZIKV-infected fetal brain tissue explants were treated with GSK717 (20 and 40 µM) or DMSO for 3 days. Viral titer determination in culture supernatants by plaque assay daily and viral genome quantification in tissues by qRT-PCR at 72 hours post-infection were performed.

For some drug assays, an MOI of 1.0 was used to infect A549 cells on coverslips with ZIKV, DENV-2 or MAYV at 1 x 10^5 cells per well in 12-well plates (Greiner) for indirect immunofluorescence of viral antigens. For the drug assays in co-infected A549 cells (DENV-2 and ZIKV or DENV-2 and MAYV), an MOI of 0.1 was used. For time-of-addition drug assays, nodosome inhibitors or DMSO were added either immediately or 12 or 24-hours after the virus absorption step. Cell supernatants were collected for viral titer determination at 24, 36, and 48-hours after addition of the compounds.

After infecting A549 cells with ZIKV, DENV-2 or MAYV (MOI=0.05-5), cells were treated with the RIPK2 inhibitor GSK583 (13) (Sigma-Aldrich) or DMSO as control for 24 hours. Furthermore, a time-of-addition assay, as described above, was performed. Cell supernatants, cells on coverslips and total cellular RNA were collected for determining viral titers by plaque assay, percentage of infected cells by indirect immunofluorescence and viral replication by qRT-PCR respectively.

GSK717 or GSK583 were used to treat SARS-CoV-2 (MOI=0.05-5) infected ACE2-SK-N-SH cells seeded into 96-well or 12-well-plates, followed by viral RNA quantification, viral titer determination or indirect immunofluorescence as described above for the arbovirus inhibition assays. Calu-3 and Huh7 cells infected with SARS-CoV-2 (MOI=0.1) were also treated with GSK583 for 24 hours before collecting the cell supernatants for viral titer determination.

As a positive control of the flaviviral inhibition in infected A549 cells (MOI=0.5-5), we used the anti-flavivirus nucleoside analog NITD008 (14) (Sigma-Aldrich) at 0.75-3 µM or DMSO alone. In the SARS-CoV-2 inhibition assays, remdesivir (15) (MedKoo Biosciences, Inc.) in infected Vero E6 cells (MOI=0.1) was used as positive control at 0.1-10 µM or DMSO as vehicle.

Immunostaining and imaging. Cells on coverslips were processed by fixing for 15 min at room temperature with 4% paraformaldehyde in PBS. Cells were washed three times in PBS and then permeabilized/blocked in Blocking buffer with 0.2% Triton-X100 and 3% BSA in PBS for 1 hour at room temperature followed by washing with PBS containing 0.3% BSA. Incubations with primary antibodies diluted 1:500 (mouse anti-Flavivirus Group Antigen 4G2, Millipore), 1:200 (mouse monoclonal anti-chikungunya capsid kindly donated by Dr. Andres Merits at University of Tartu, Estonia)(16), or 1:250 (mouse monoclonal anti-spike SARS-CoV/SARS-CoV-2, GenTex) in Blocking buffer were carried out at room temperature for 1.5 hour followed by three washes in Washing buffer (0.02% Triton-X100 with 0.3% BSA and PBS).

Samples were then incubated with secondary antibodies (1:1000) in Blocking buffer containing 1 µg/mL of DAPI for 1 hour at room temperature followed by three washes in Washing buffer. Secondary antibodies (Invitrogen) were Alexa Fluor 488 anti-mouse. Confocal images of cells on coverslips were acquired using an Olympus 1x81 spinning disk confocal microscope (Tokyo, Japan) and images were analyzed using Volocity 6.2.1 software. A set of confocal imaging was

acquired using a Cytation 5 Cell Imaging Multi-Mode Reader and analyzed using Gen5 software (Biotek). Total and antigen-positive cells were counted in 10 image fields per well, and the percentage of infected cells was obtained.

Supplemental Figure legends

Fig S1. Inflammasome induction by human recombinant IFN-α and NOD2 silencing in HFAs. HFAs were treated with human recombinant IFN-α for 4, 8 and 12 hours after which relative expression of inflammasome genes gasdermin D (*GSDMD*) (**A**), caspase 1 (*Casp1*) (**B**), guanylate binding protein 5 (*GBP5*) (**C**) and NOD-like receptor family CARD domain containing 5 (*NLRC5*) (**D**) were determined. (**E**) HFAs were transfected with NOD2-specific or non-silencing siRNAs for 24-hours followed by ZIKV infection (MOI=0.05). Total cellular RNA was collected at 48 hours post-infection for *NOD2* gene quantitation by qRT-PCR. Relative levels of *NOD2* is shown. (**F**) Cellular ATP levels in uninfected HFAs were determined using the CellTiter-Glo assay kit after *NOD2* silencing for 72 hours. Values are expressed as the mean of three independent experiments. Error bars represent standard errors of the mean. $*P < 0.05$, $**P < 0.01$, and $***P < 0.001$, by the Student *t* test.

Fig S2. NOD2 blocking drug GSK717 displays anti-ZIKV activity in different cell types. Human primary embryonic pulmonary fibroblasts (HEL-18) were treated with GSK717 or DMSO as control for 72 hours after ZIKV infection with MOI of 0.05 and 5. ZIKV titers are shown as relative fold with MOI of 0.05 (**A)** and 5 (**B**) at 48-72 hours post-infection and as PFU/mL with MOI of 0.05 (**C**) at 48 hours post-infection. ZIKV titers as relative fold in A549 (**D**), U251 (**E**) and Huh7 (**F**) cells after 48 hours of infection (MOI=0.05-5) with and without GSK717 treatment are shown. (**G**) Viral titers as relative fold in A549 cells infected with ZIKV (MOI=0.1) for 0, 12 or 24 hours followed by GSK717 drug or DMSO addition for 48, 36 or 24 hours respectively are

shown. Values are expressed as the mean of three independent experiments. Error bars represent standard errors of the mean. *$P < 0.05$, **$P < 0.01$, and ***$P < 0.001$, by the Student *t* test.

Fig S3. Anti-NOD2 drug is not cytotoxic in human primary cells and cell lines. (**A**) Cellular ATP levels, measured by the CellTiter-Glo assay kit, of uninfected HFAs treated with the GSK717 or DMSO for 72 hours are shown. Cellular ATP measurements in the A549 (**B**), U251 (**C**), Huh7 (**D**) and ACE2-SK-N-SH (**E**) cell lines after 48 hours of GSK717 or DMSO treatment are presented. Values are expressed as the mean of three independent experiments. Error bars represent standard errors of the mean.

Fig S4. GSK717 blocks the spread of DENV-2. (**A**) Representative confocal imaging (20X) of DENV-2 infected cells treated with GSK717. A549 cells were infected with DENV-2 (MOI=1) followed by treatment with DMSO or GSK717 at 20 or 40 µM for 48 hours before fixation and immunostaining. DENV-infected cells were detected using mouse monoclonal antibody (4G2) to envelope protein and Alexa Fluor 488 donkey anti-mouse. Nuclei were stained with DAPI. Images were acquired using a spinning disk confocal microscope equipped with Volocity 6.2.1 software. (**B**) Infected cells were counted in 10 different fields for GSK717 and DMSO treated samples. Values are expressed as the mean of three independent experiments. Error bars represent standard errors of the mean. **$P < 0.01$, by the Student *t* test.

Fig S5. RIPK2 inhibitor GSK583 suppresses arboviral replication at sub-cytotoxic concentrations. A549 cells were infected with MAYV (MOI=0.1) and treated with RIPK2 inhibitor GSK583 (30 µM) or DMSO. Relative fold of titers (**A**) and viral genome (**B**) at 12- and 24-hours post-infection is shown. (**C**) A549 cells infected separately with arboviruses at low (0.05) and high MOI (5) were treated with GSK583 (30 µM) or DMSO for 24 hours before supernatant collection for plaque assays. Viral titers as relative fold is shown. (**D**) Cellular ATP measurements

by the CellTiter-Glo assay kit in uninfected A549 after 24 hours of GSK583 or DMSO treatment are shown. Values are expressed as the mean of three independent experiments. Error bars represent standard errors of the mean. *$P < 0.05$, **$P < 0.01$, and ***$P < 0.001$ by the Student *t* test.

Fig S6. RIPK2 inhibitor GSK583 blocks the spread of arboviruses. (**A**) Representative confocal imaging (20X) of GSK583 effect on MAYV-infected A549 cells. Cells were infected with MAYV, ZIKV or DENV (MOI=1) and then treated with GSK583 (15 or 30 µM) for 24 hours before processing for indirect immunofluorescence. Infected cells were identified using mouse anti-alphavirus capsid (MAYV) or anti-flavivirus envelope 4G2 (ZIKV and DENV-2) and Alexa Fluor 488 donkey anti-mouse. Nuclei were stained with DAPI. Images of MAYV-infected cells were acquired using a Cytation 5 Cell Imaging Multi-Mode Reader and analyzed using Gen5 software (Biotek) while images of flavivirus infected cells (ZIKV and DENV-2) were acquired using a spinning disk confocal microscope with Volocity 6.2.1 software. Infected cells were determined by counting within 10 different fields for each sample of MAYV (**B**), ZIKV (**C**) and DENV-2 (**D**). Values are expressed as the mean of three independent experiments. Error bars represent standard errors of the mean. *$P < 0.05$, **$P < 0.01$, and ***$P < 0.001$, by the Student *t* test.

Fig S7. RIPK2 inhibitor blocks the infection by and spread of SARS-CoV-2 in ACE2-SK-N-SH. (**A**) ACE2-SK-N-SH were infected with SARS-CoV-2 (MOI=0.1) followed by treatment with 30 µM of GSK583 or DMSO. Cell supernatants were collected at 12- and 24-hours post-infection for plaque assay. Viral titers as PFU/mL is shown. (**B**) The same drug concentration was also added at 0 and 24 hours after infection with SARS-CoV-2 (MOI=0.1) to determine titers (PFU/mL) in ACE2-SK-N-SH supernatants 24 hours post-treatment. (**C**) Representative confocal imaging

(20X) of ACE2-SK-N-SH infected with SARS-CoV-2 (MOI=1) and treated with GSK583 or DMSO for 24 hours. After fixation, coronavirus-infected cells were stained using mouse monoclonal antibody to SARS spike protein as primary antibody and secondary antibodies were Alexa Fluor 488 donkey anti-mouse. Nuclei were stained with DAPI. Confocal images were acquired using a spinning disk confocal microscope with Volocity 6.2.1 software. (**D**) Cells were counted in 10 different fields for quantitation of infected cells after GSK583 or DMSO treatment. Values are expressed as the mean of three independent experiments. Error bars represent standard errors of the mean. *$P < 0.05$, **$P < 0.01$, and ***$P < 0.001$, by the Student *t* test.

Fig S8. GSK583 suppresses SARS-CoV-2 release at subtoxic concentrations. Calu-3 (**A**) and Huh7 (**B**) cells were infected with SARS-CoV-2 at the MOI of 0.1 and treated with GSK583 or DMSO as control for 24 hours after which cell supernatants were collected for plaque assay. Viral titers as relative fold is shown. Cellular ATP measurements using the CellTiter-Glo assay kit are shown at the 24-hour time point after GSK583 or DMSO treatment in uninfected ACE2-SK-N-SH (**C**), Calu-3 (**D**), and Huh7 (**E**) cells. Values are expressed as the mean of three independent experiments. Error bars represent standard errors of the mean. *$P < 0.05$, **$P < 0.01$, and ***$P < 0.001$, by the Student *t* test.

SUPPLEMENTAL REFERENCES

1. Lanciotti RS, Lambert AJ, Holodniy M, Saavedra S, Signor Ldel C. 2016. Phylogeny of Zika Virus in Western Hemisphere, 2015. Emerg Infect Dis 22:933-5.
2. Limonta D, Branton W, Wong CP, Saito L, Power C, Hobman TC. 2020. Use of Primary Human Fetal Astrocytes and Tissue Explants as Ex Vivo Models to Study Zika Virus Infection of the Developing Brain. Methods Mol Biol 2142:251-259.

3. Megyeri K, Berencsi K, Halazonetis TD, Prendergast GC, Gri G, Plotkin SA, Rovera G, Gönczöl E. 1999. Involvement of a p53-dependent pathway in rubella virus-induced apoptosis. Virology 259:74-84.

4. Capitanio JS, Montpetit B, Wozniak RW. 2017. Human Nup98 regulates the localization and activity of DExH/D-box helicase DHX9. Elife 6.

5. Schoggins JW, Wilson SJ, Panis M, Murphy MY, Jones CT, Bieniasz P, Rice CM. 2011. A diverse range of gene products are effectors of the type I interferon antiviral response. Nature 472:481-5.

6. Li W, Moore MJ, Vasilieva N, Sui J, Wong SK, Berne MA, Somasundaran M, Sullivan JL, Luzuriaga K, Greenough TC, Choe H, Farzan M. 2003. Angiotensin-converting enzyme 2 is a functional receptor for the SARS coronavirus. Nature 426:450-4.

7. Guan B, Wang TL, Shih IM. 2011. ARID1A, a factor that promotes formation of SWI/SNF-mediated chromatin remodeling, is a tumor suppressor in gynecologic cancers. Cancer Res 71:6718-27.

8. Balm MN, Lee CK, Lee HK, Chiu L, Koay ES, Tang JW. 2012. A diagnostic polymerase chain reaction assay for Zika virus. J Med Virol 84:1501-5.

9. Chien LJ, Liao TL, Shu PY, Huang JH, Gubler DJ, Chang GJ. 2006. Development of real-time reverse transcriptase PCR assays to detect and serotype dengue viruses. J Clin Microbiol 44:1295-304.

10. Waggoner JJ, Rojas A, Mohamed-Hadley A, de Guillén YA, Pinsky BA. 2018. Real-time RT-PCR for Mayaro virus detection in plasma and urine. J Clin Virol 98:1-4.

11. Zhou P, Yang XL, Wang XG, Hu B, Zhang L, Zhang W, Si HR, Zhu Y, Li B, Huang CL, Chen HD, Chen J, Luo Y, Guo H, Jiang RD, Liu MQ, Chen Y, Shen XR, Wang X, Zheng

XS, Zhao K, Chen QJ, Deng F, Liu LL, Yan B, Zhan FX, Wang YY, Xiao GF, Shi ZL. 2020. A pneumonia outbreak associated with a new coronavirus of probable bat origin. Nature 579:270-273.

12. Rickard DJ, Sehon CA, Kasparcova V, Kallal LA, Zeng X, Montoute MN, Chordia T, Poore DD, Li H, Wu Z, Eidam PM, Haile PA, Yu J, Emery JG, Marquis RW, Gough PJ, Bertin J. 2013. Identification of benzimidazole diamides as selective inhibitors of the nucleotide-binding oligomerization domain 2 (NOD2) signaling pathway. PLoS One 8:e69619.

13. Haile PA, Votta BJ, Marquis RW, Bury MJ, Mehlmann JF, Singhaus R, Charnley AK, Lakdawala AS, Convery MA, Lipshutz DB, Desai BM, Swift B, Capriotti CA, Berger SB, Mahajan MK, Reilly MA, Rivera EJ, Sun HH, Nagilla R, Beal AM, Finger JN, Cook MN, King BW, Ouellette MT, Totoritis RD, Pierdomenico M, Negroni A, Stronati L, Cucchiara S, Ziółkowski B, Vossenkämper A, MacDonald TT, Gough PJ, Bertin J, Casillas LN. 2016. The Identification and Pharmacological Characterization of 6-(tert-Butylsulfonyl)-N-(5-fluoro-1H-indazol-3-yl)quinolin-4-amine (GSK583), a Highly Potent and Selective Inhibitor of RIP2 Kinase. J Med Chem 59:4867-80.

14. Yin Z, Chen YL, Schul W, Wang QY, Gu F, Duraiswamy J, Kondreddi RR, Niyomrattanakit P, Lakshminarayana SB, Goh A, Xu HY, Liu W, Liu B, Lim JY, Ng CY, Qing M, Lim CC, Yip A, Wang G, Chan WL, Tan HP, Lin K, Zhang B, Zou G, Bernard KA, Garrett C, Beltz K, Dong M, Weaver M, He H, Pichota A, Dartois V, Keller TH, Shi PY. 2009. An adenosine nucleoside inhibitor of dengue virus. Proc Natl Acad Sci U S A 106:20435-9.

15. Pruijssers AJ, George AS, Schäfer A, Leist SR, Gralinksi LE, Dinnon KH, Yount BL, Agostini ML, Stevens LJ, Chappell JD, Lu X, Hughes TM, Gully K, Martinez DR, Brown AJ, Graham RL, Perry JK, Du Pont V, Pitts J, Ma B, Babusis D, Murakami E, Feng JY, Bilello JP, Porter DP, Cihlar T, Baric RS, Denison MR, Sheahan TP. 2020. Remdesivir Inhibits SARS-CoV-2 in Human Lung Cells and Chimeric SARS-CoV Expressing the SARS-CoV-2 RNA Polymerase in Mice. Cell Rep 32:107940.

16. Goh LYH, Hobson-Peters J, Prow NA, Gardner J, Bielefeldt-Ohmann H, Suhrbier A, Hall RA. 2015. Monoclonal antibodies specific for the capsid protein of chikungunya virus suitable for multiple applications. J Gen Virol 96:507-512.

FIG S1

A

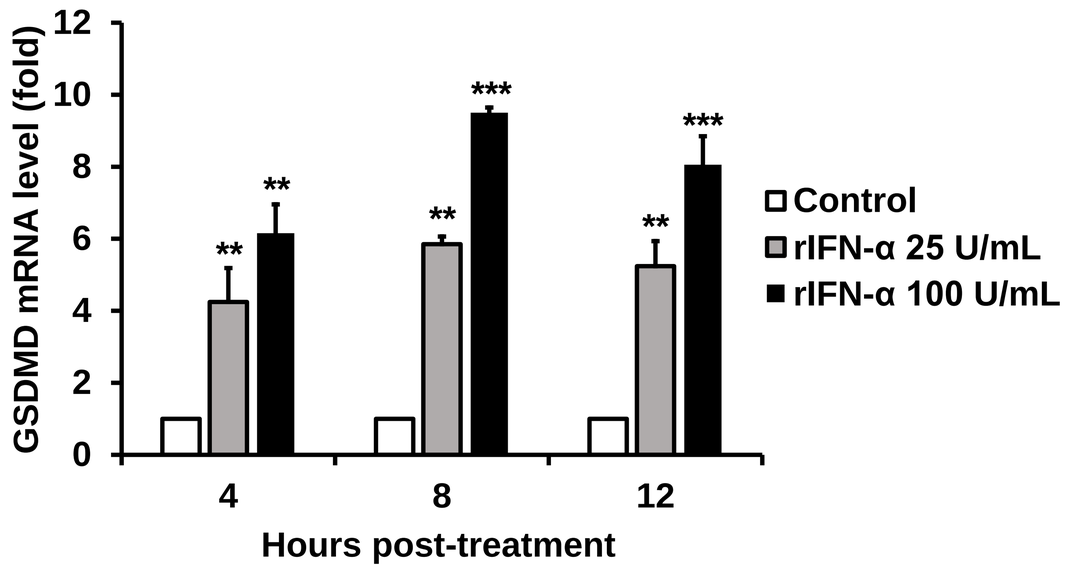

B

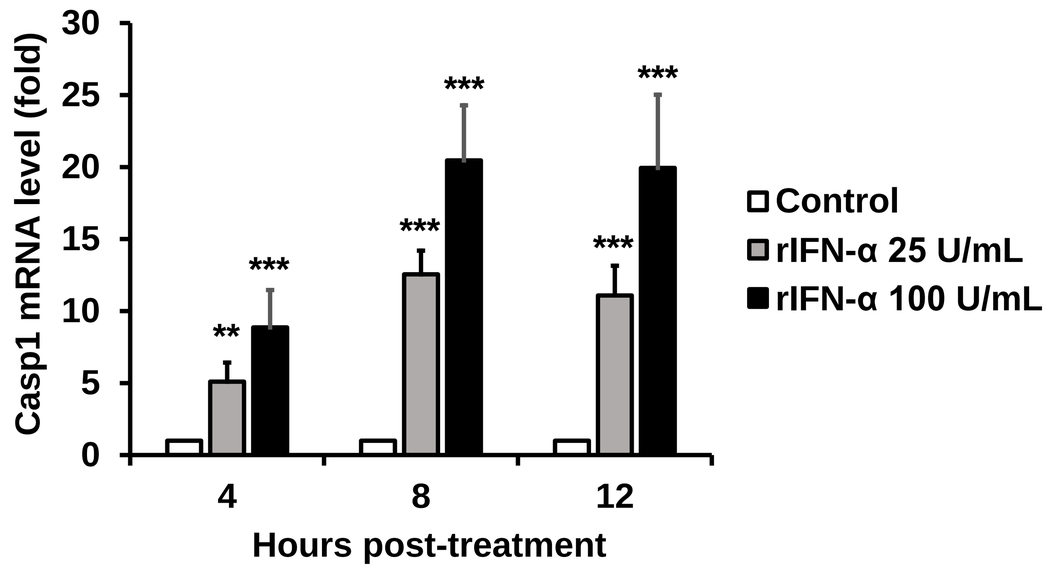

C

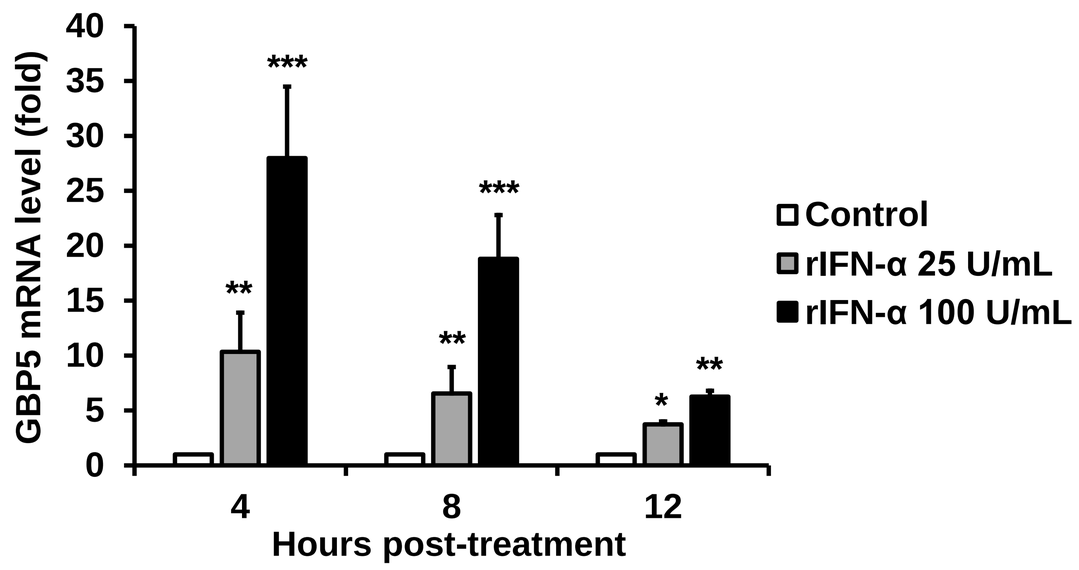

D

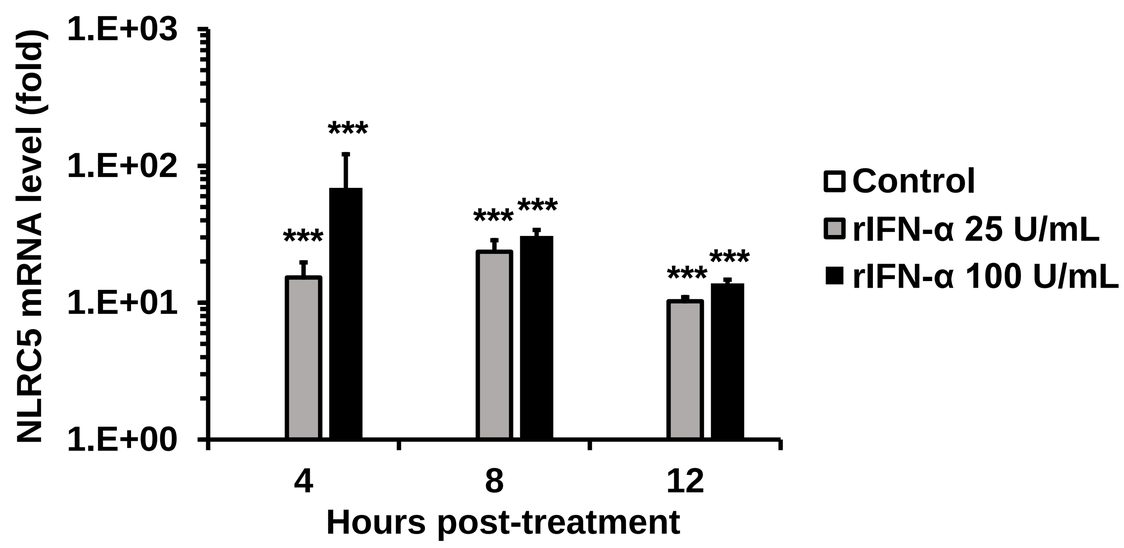

E

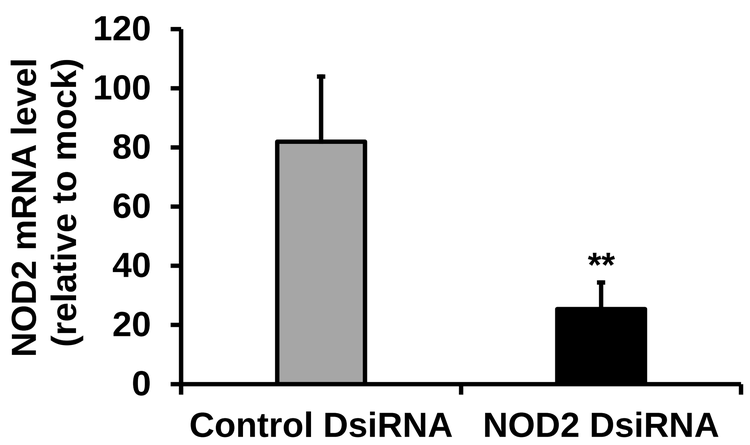

F

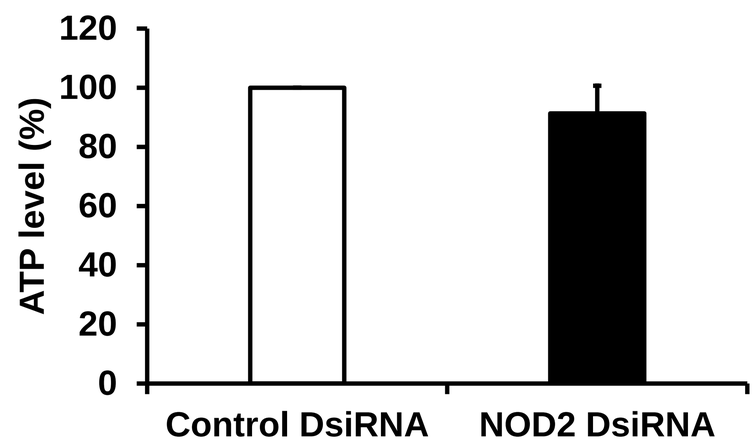

FIG S2

A

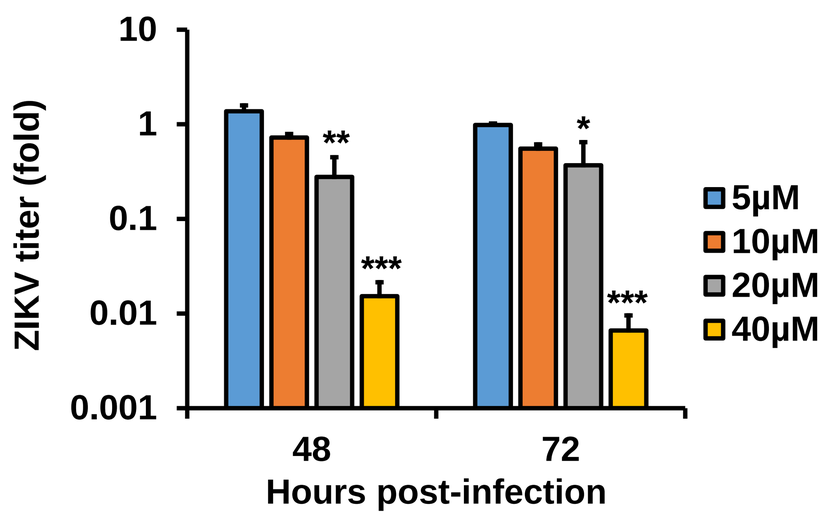

B

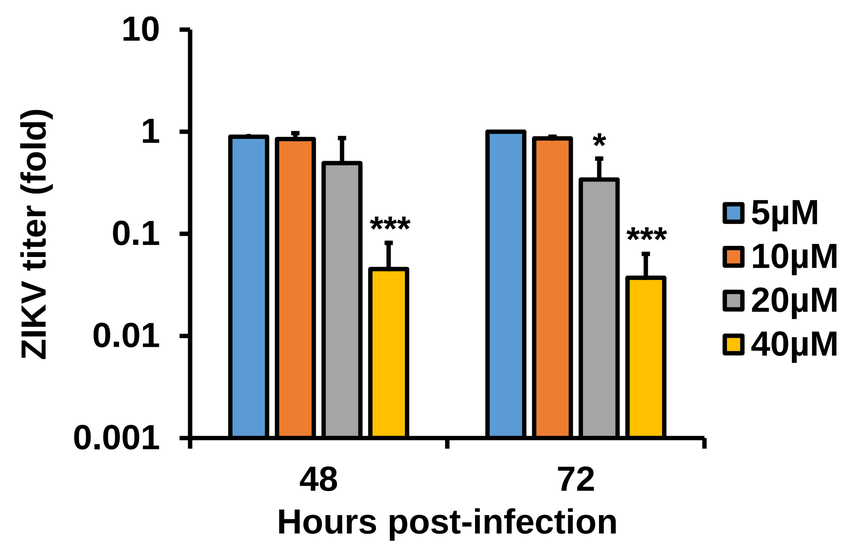

C

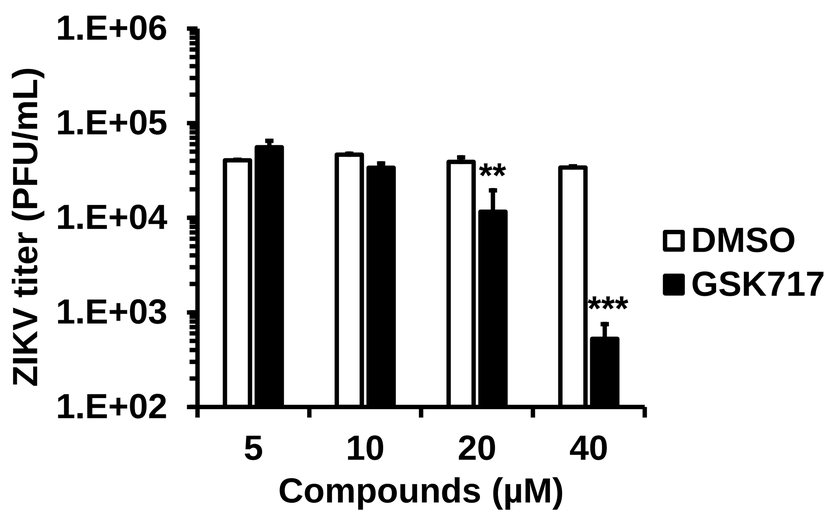

D

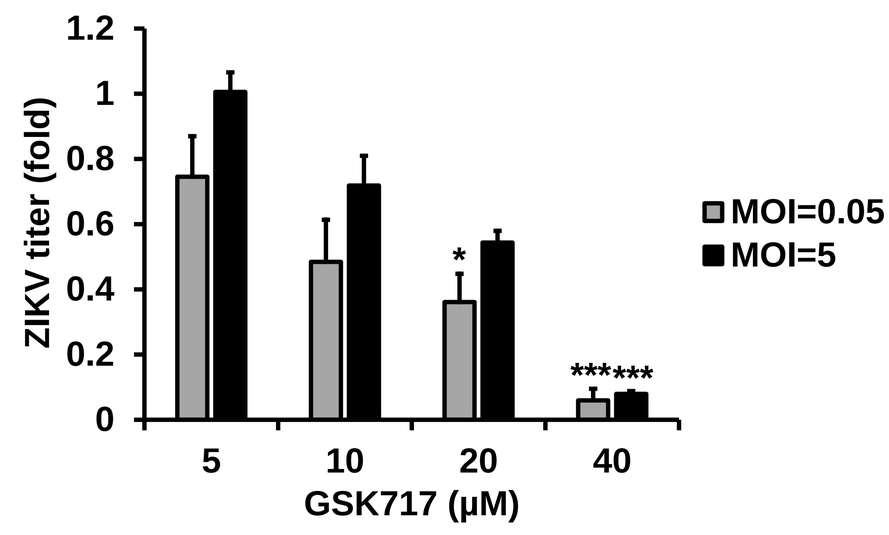

E

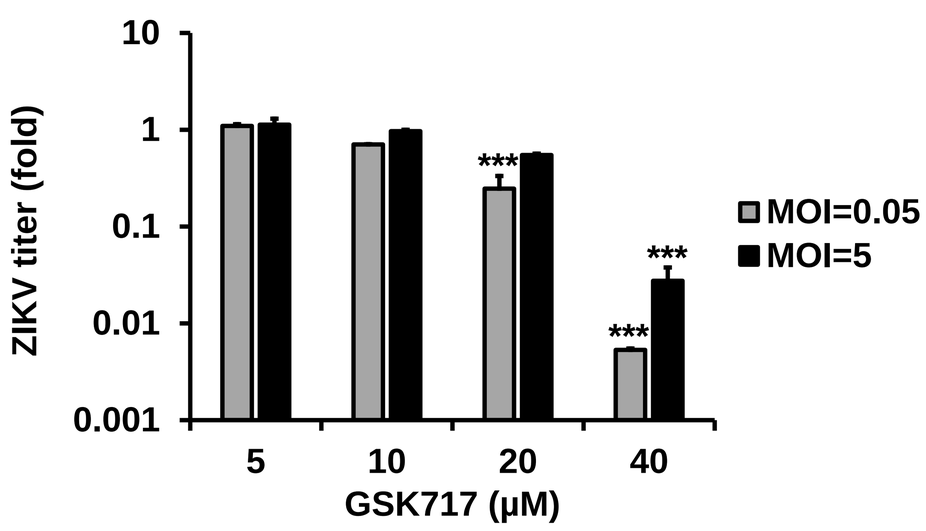

F

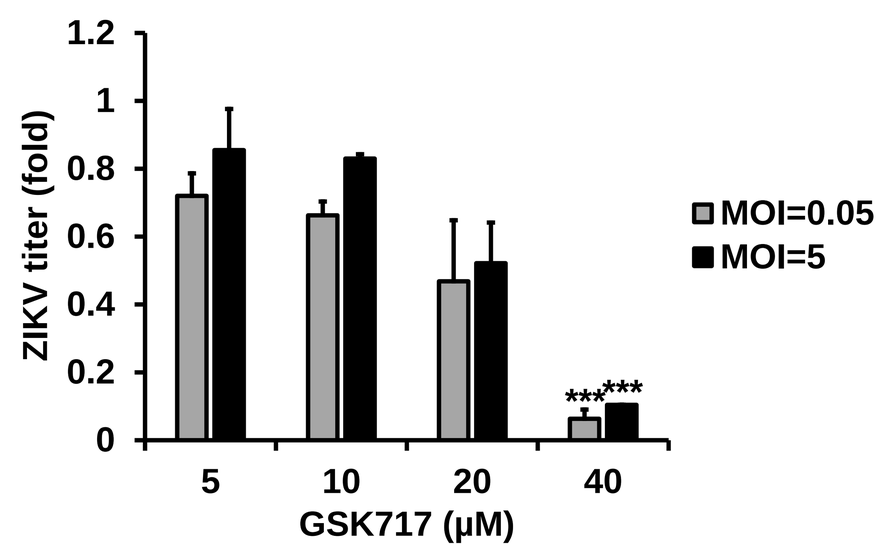

G

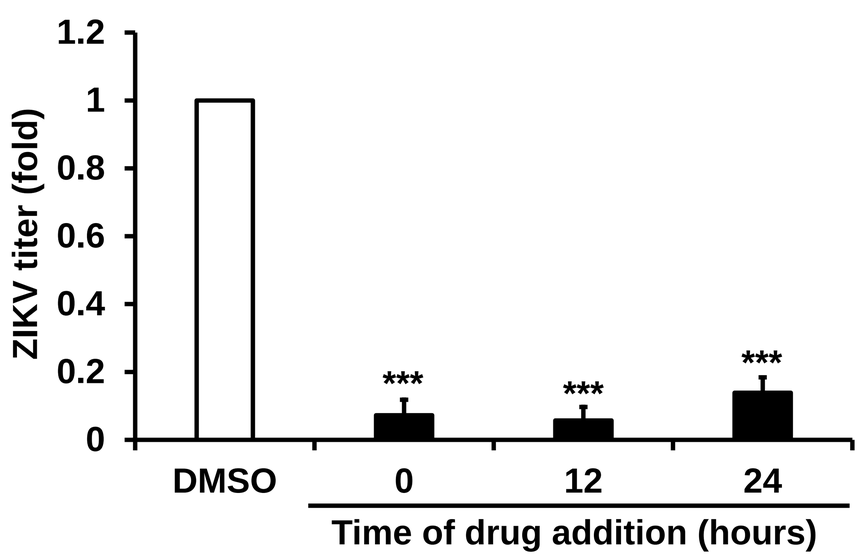

FIG S3

A

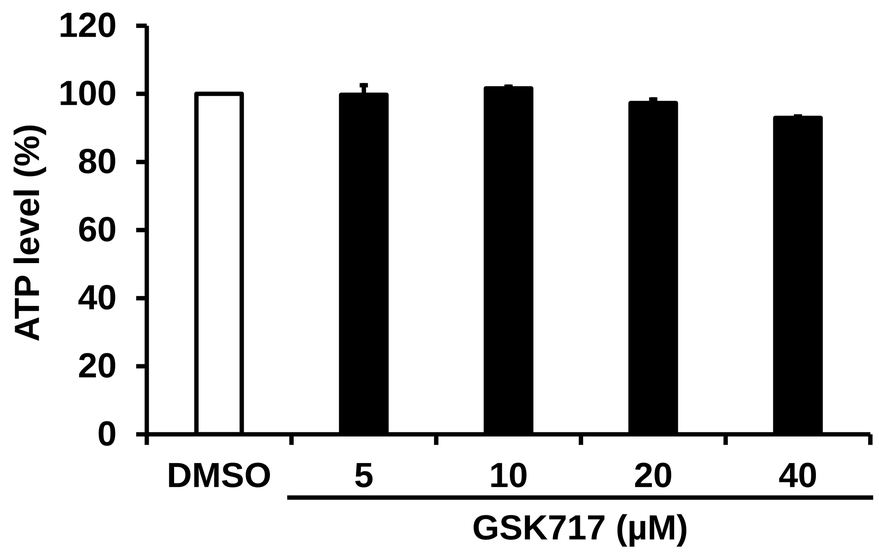
120
100
80
60
40
20
0
ATP level (%)
DMSO
5
10
20
40
GSK717 (μM)

B

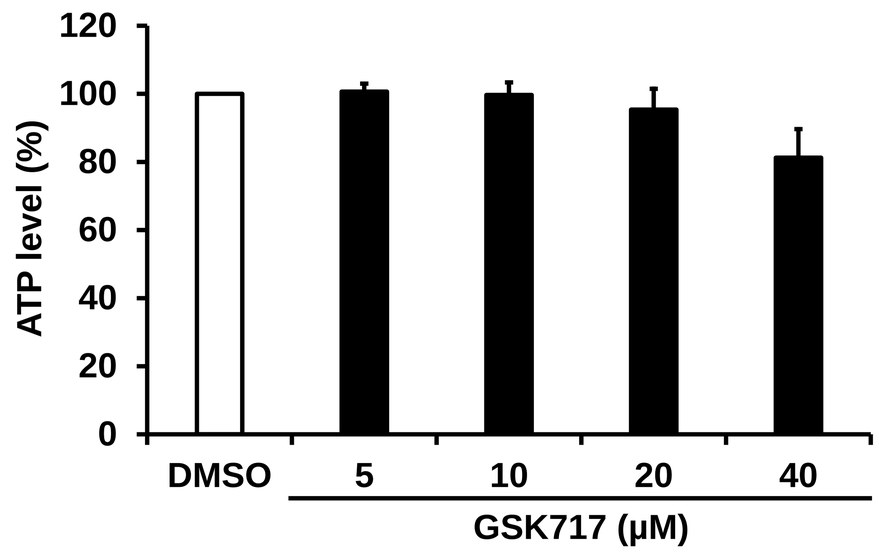
120
100
80
60
40
20
0
ATP level (%)
DMSO
5
10
20
40
GSK717 (μM)

C

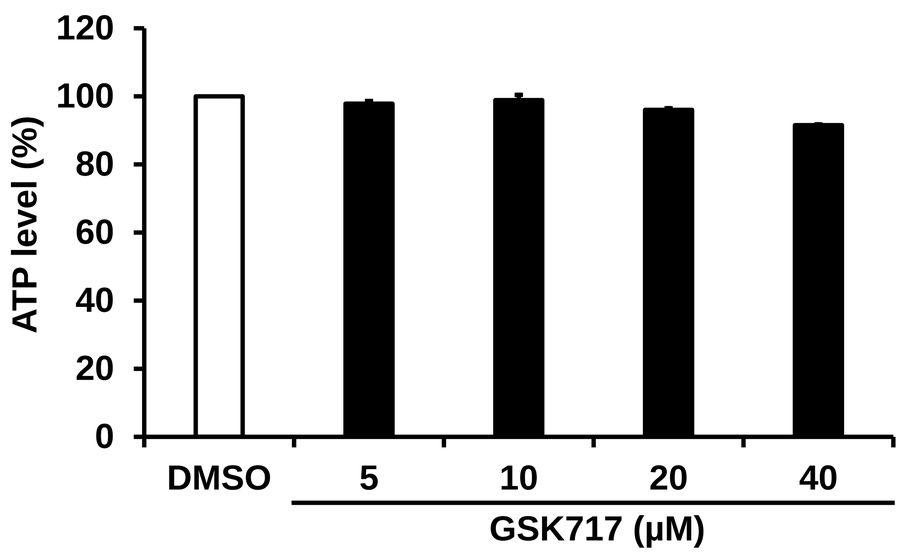
120
100
80
60
40
20
0
ATP level (%)
DMSO
5
10
20
40
GSK717 (μM)

D

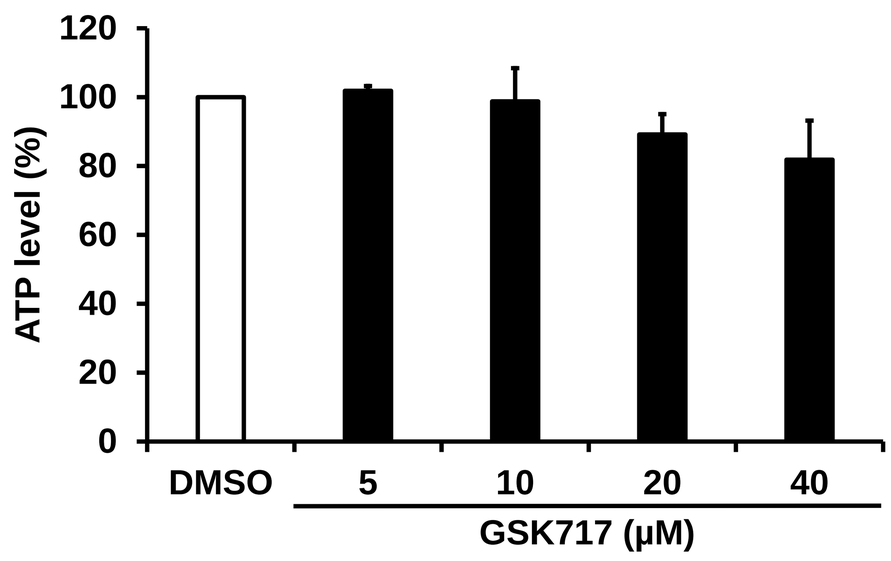
120
100
80
60
40
20
0
ATP level (%)
DMSO
5
10
20
40
GSK717 (μM)

E

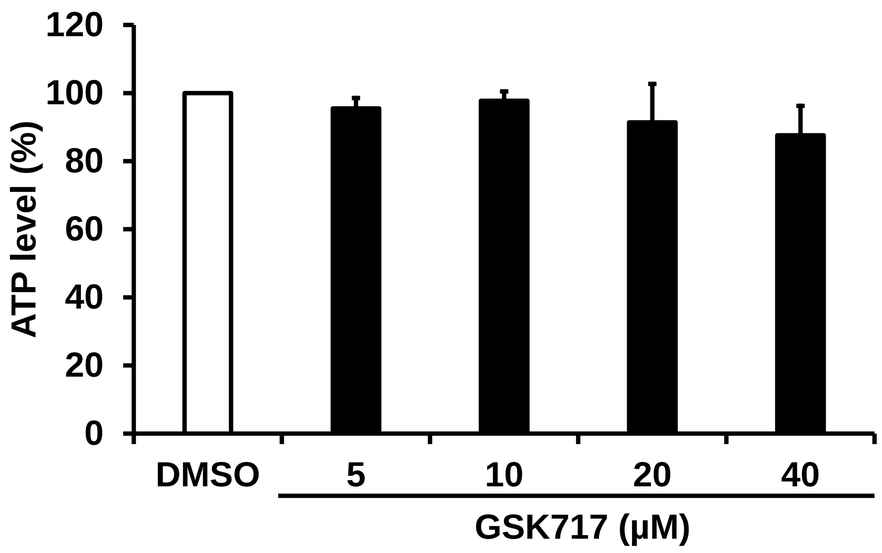
120
100
80
60
40
20
0
ATP level (%)
DMSO
5
10
20
40
GSK717 (μM)

FIG S4

A

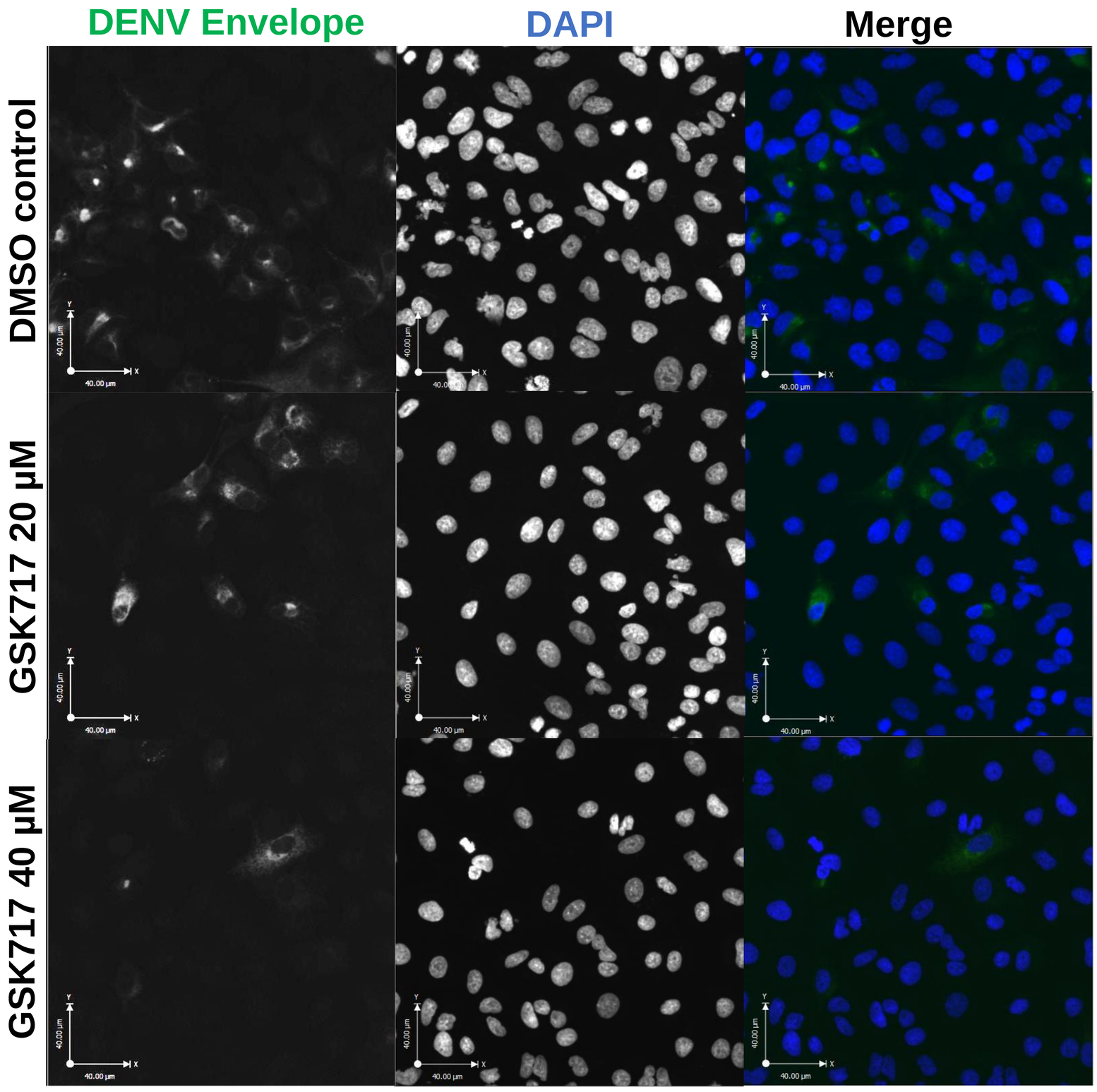
DENV Envelope
DAPI
Merge
DMSO control
GSK717 20 µM
GSK717 40 µM

B

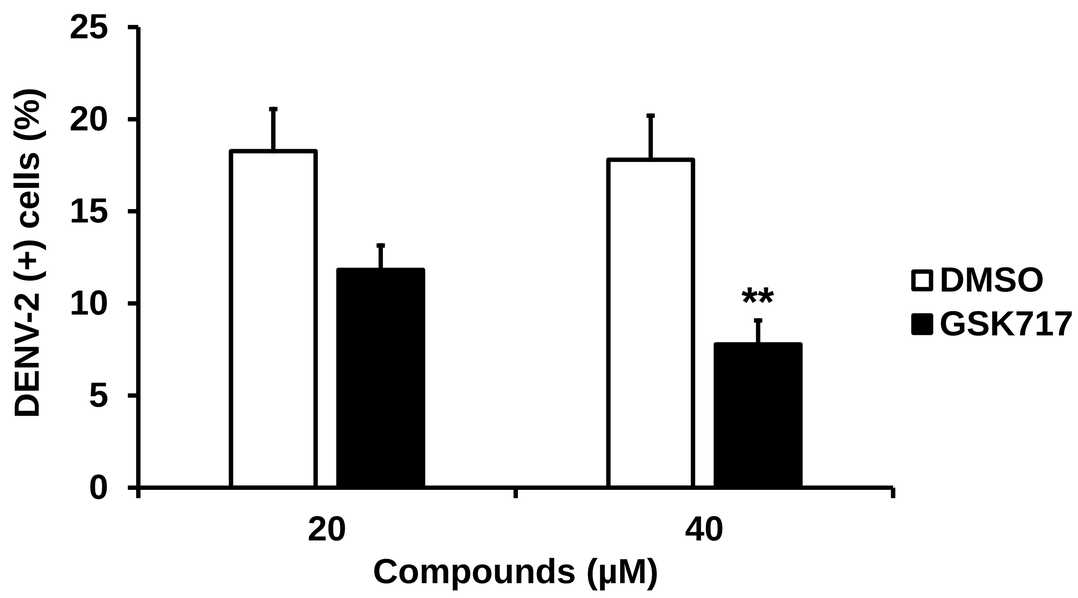
DENV-2 (+) cells (%)
25
20
15
10
5
0
**
DMSO
GSK717
20
40
Compounds (µM)

FIG S5

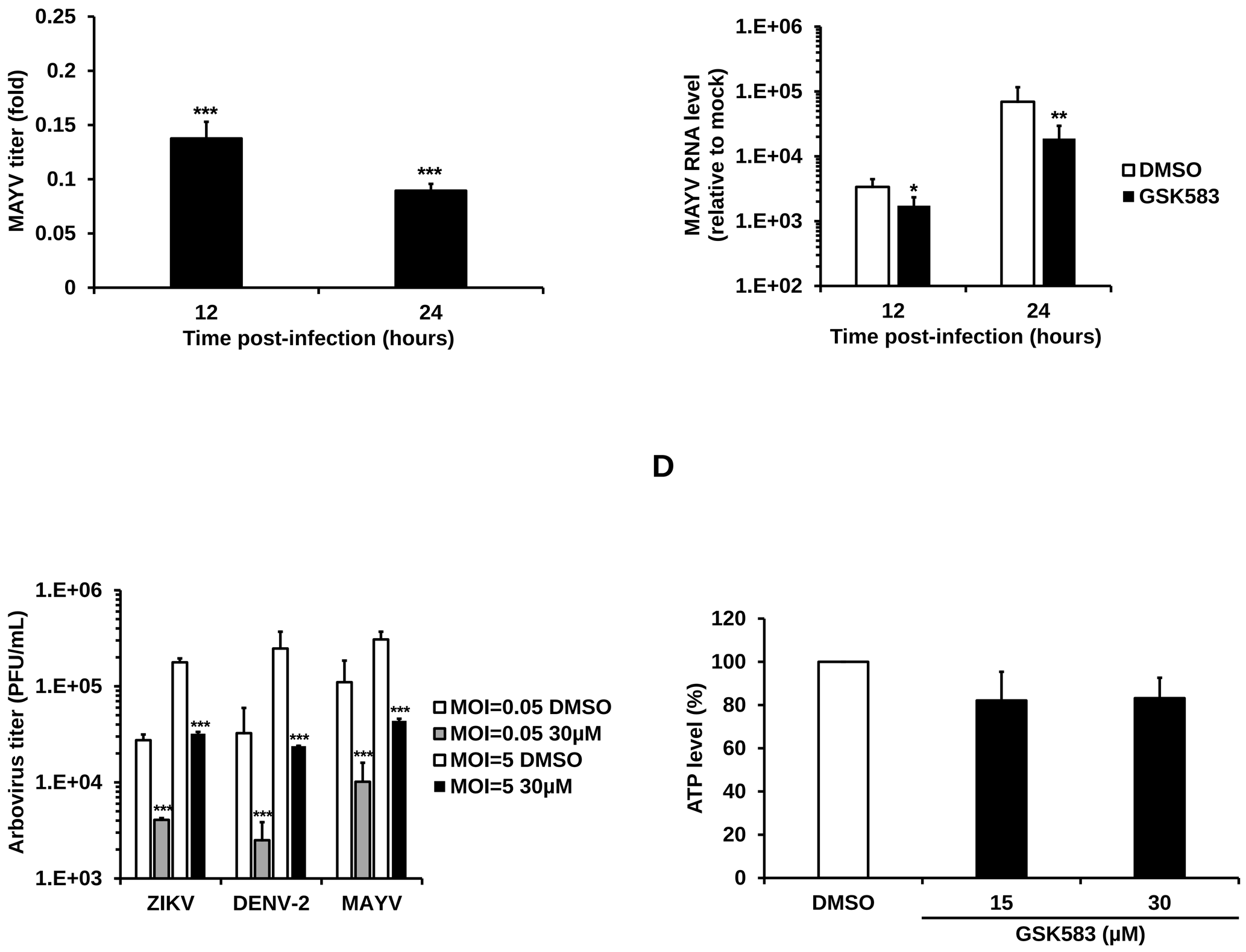
A
MAYV titer (fold)
0.25
0.2
0.15
0.1
0.05
0
***
***
12
24
Time post-infection (hours)
B
MAYV RNA level (relative to mock)
1.E+06
1.E+05
1.E+04
1.E+03
1.E+02
*
**
12
24
Time post-infection (hours)
DMSO
GSK583
C
Arbovirus titer (PFU/mL)
1.E+06
1.E+05
1.E+04
1.E+03
***
ZIKV
DENV-2
MAYV
MOI=0.05 DMSO
MOI=0.05 30μM
MOI=5 DMSO
MOI=5 30μM
D
ATP level (%)
120
100
80
60
40
20
0
DMSO
15
30
GSK583 (μM)

FIG S6

A

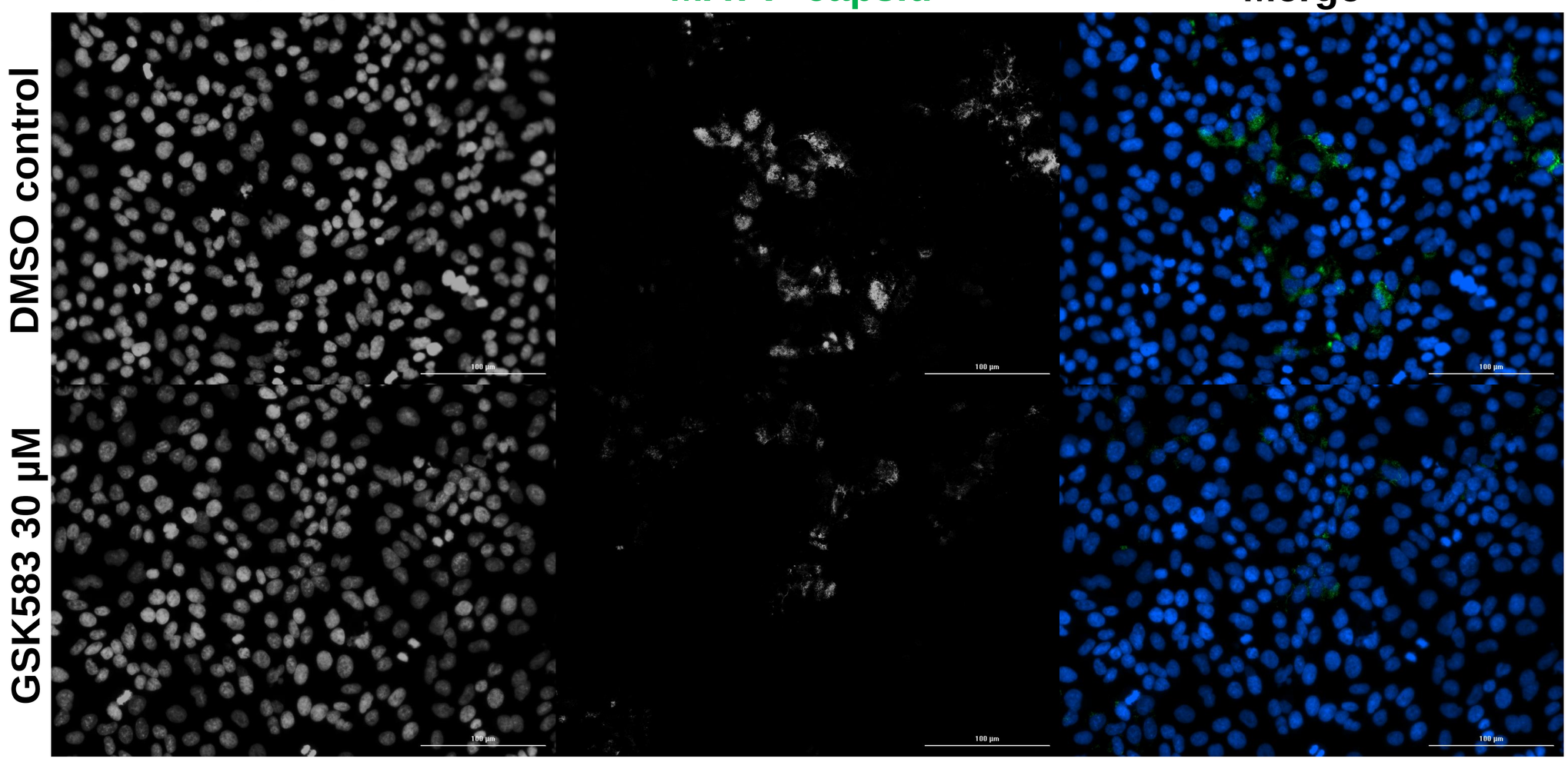
DAPI
MAYV capsid
Merge
DMSO control
GSK583 30 μM
100 μm

B

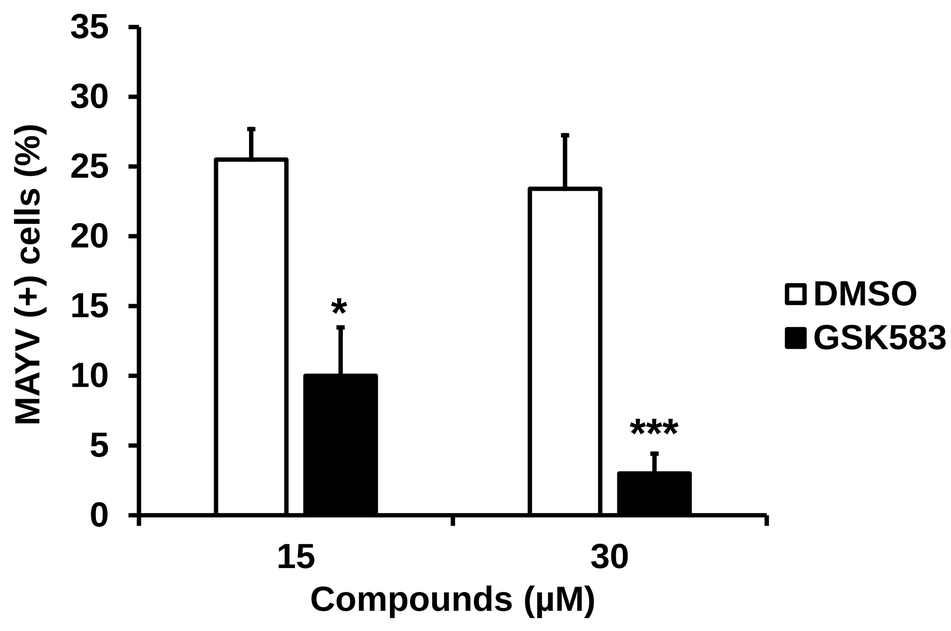
MAYV (+) cells (%)
35
30
25
20
15
10
5
0
*
***
15
30
Compounds (μM)
DMSO
GSK583

C

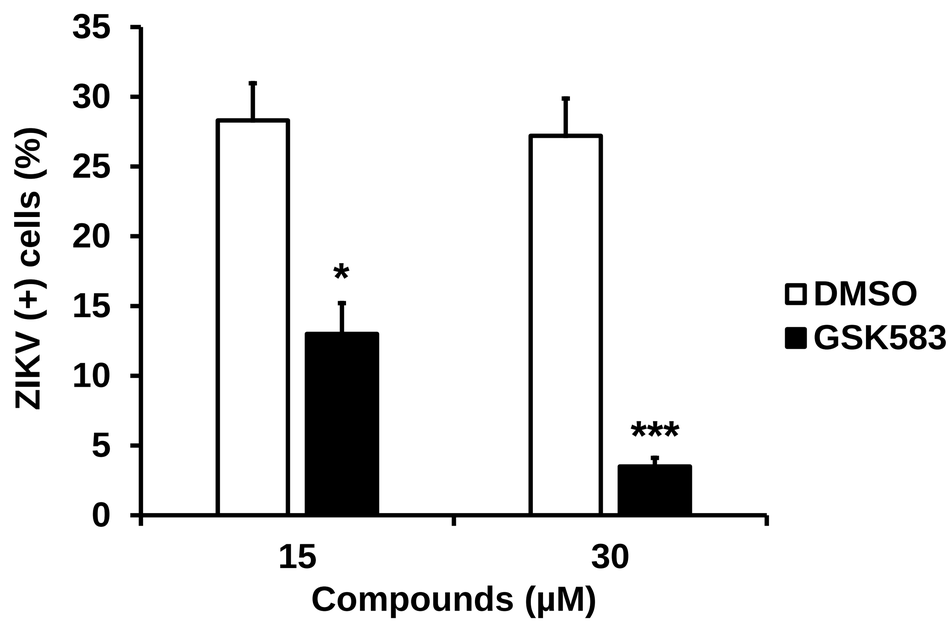
ZIKV (+) cells (%)
35
30
25
20
15
10
5
0
*
***
15
30
Compounds (μM)
DMSO
GSK583

D

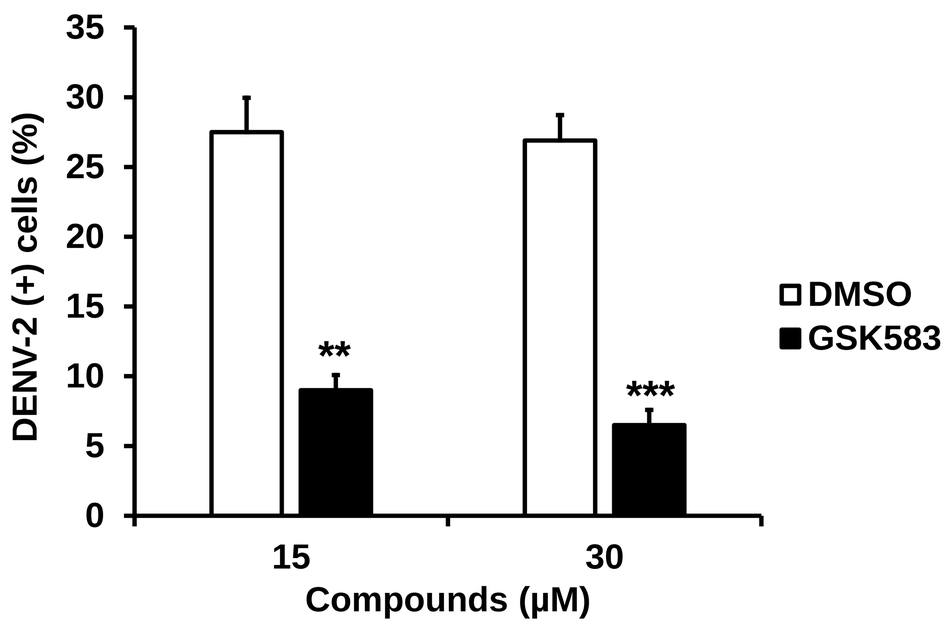
DENV-2 (+) cells (%)
35
30
25
20
15
10
5
0
**
***
15
30
Compounds (μM)
DMSO
GSK583

FIG S7

A

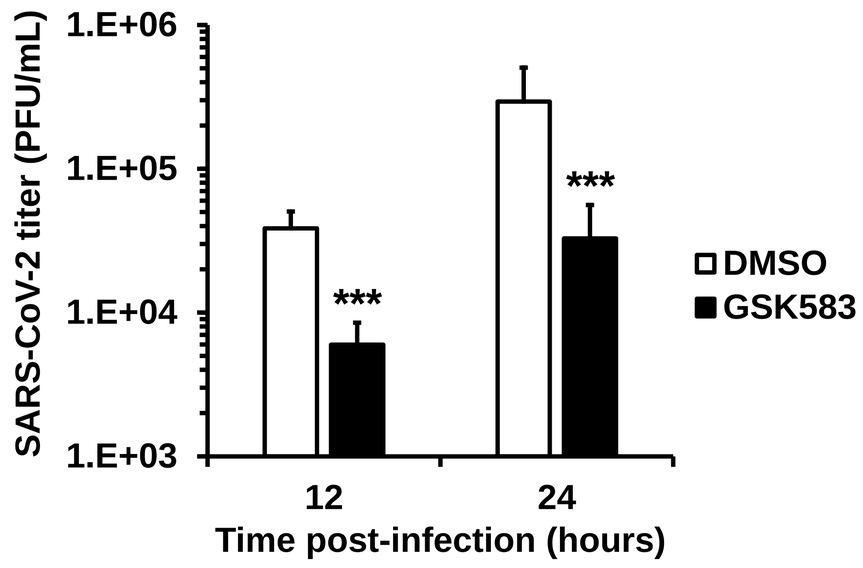
SARS-CoV-2 titer (PFU/mL)
1.E+06
1.E+05
1.E+04
1.E+03
***
***
12
24
Time post-infection (hours)
DMSO
GSK583

B

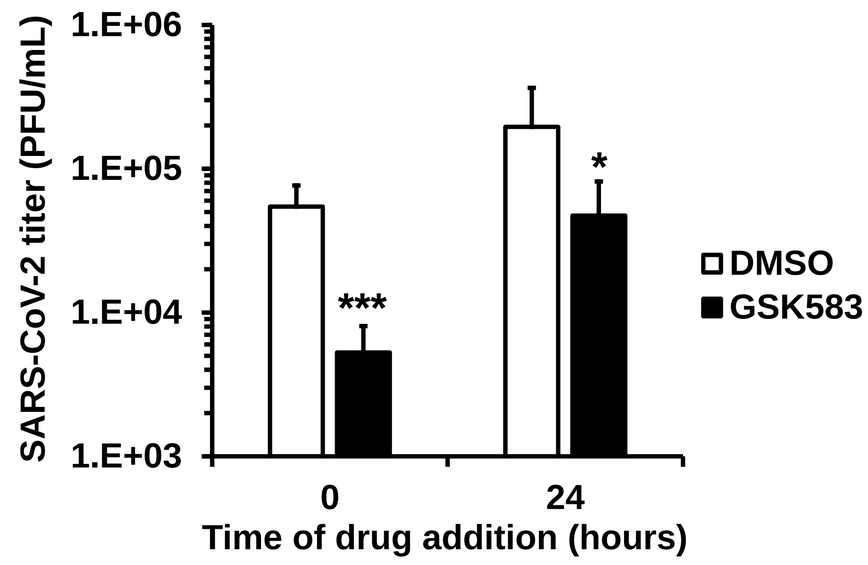
SARS-CoV-2 titer (PFU/mL)
1.E+06
1.E+05
1.E+04
1.E+03
***
*
0
24
Time of drug addition (hours)
DMSO
GSK583

C

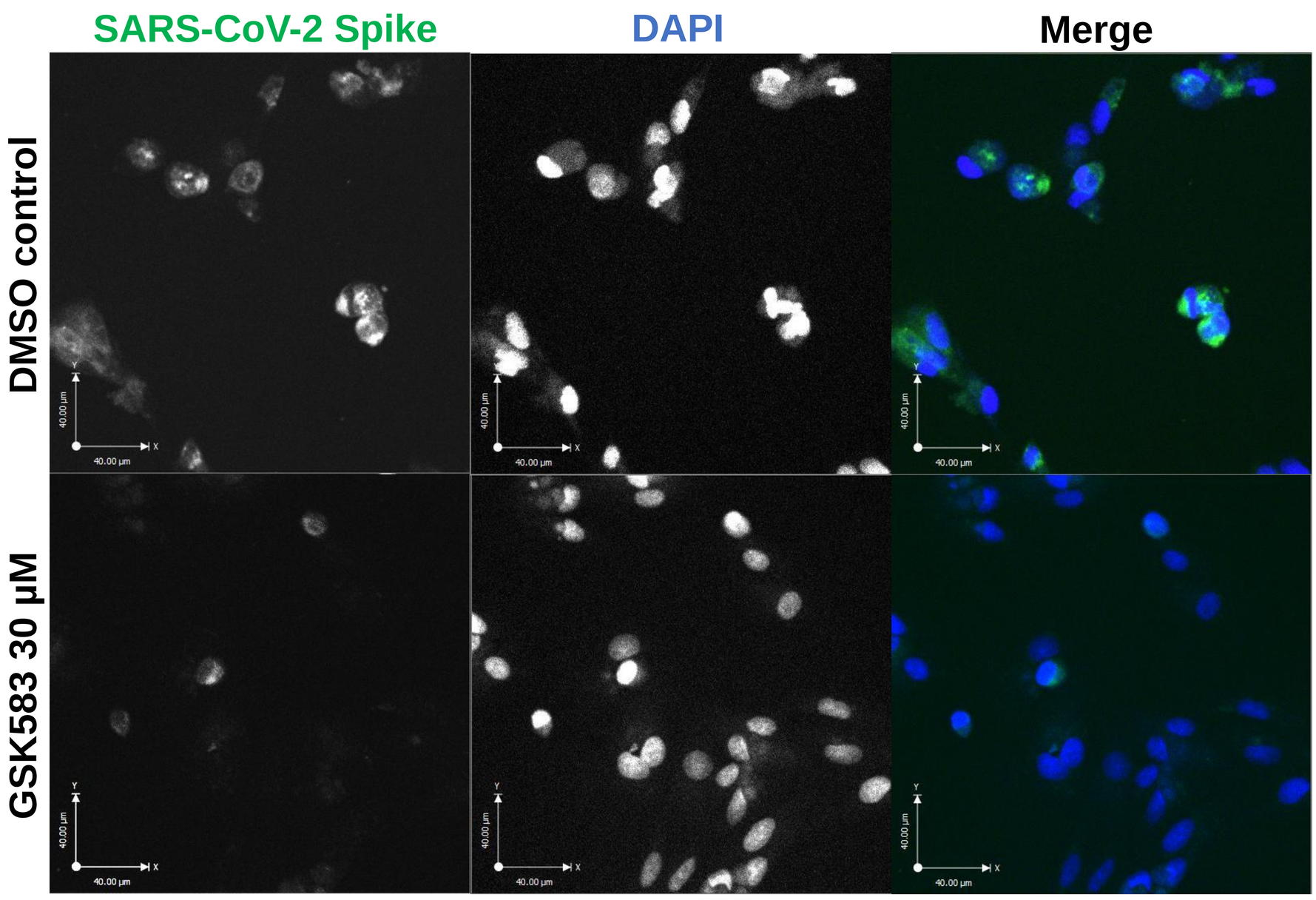
SARS-CoV-2 Spike
DAPI
Merge
DMSO control
GSK583 30 µM

D

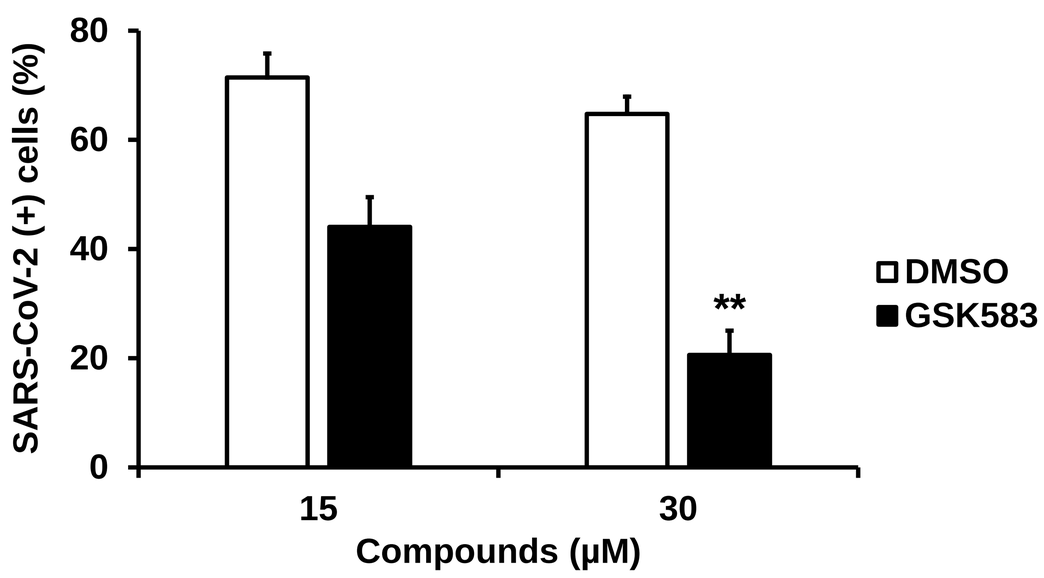
SARS-CoV-2 (+) cells (%)
80
60
40
20
0
**
15
30
Compounds (µM)
DMSO
GSK583

FIG S8

A

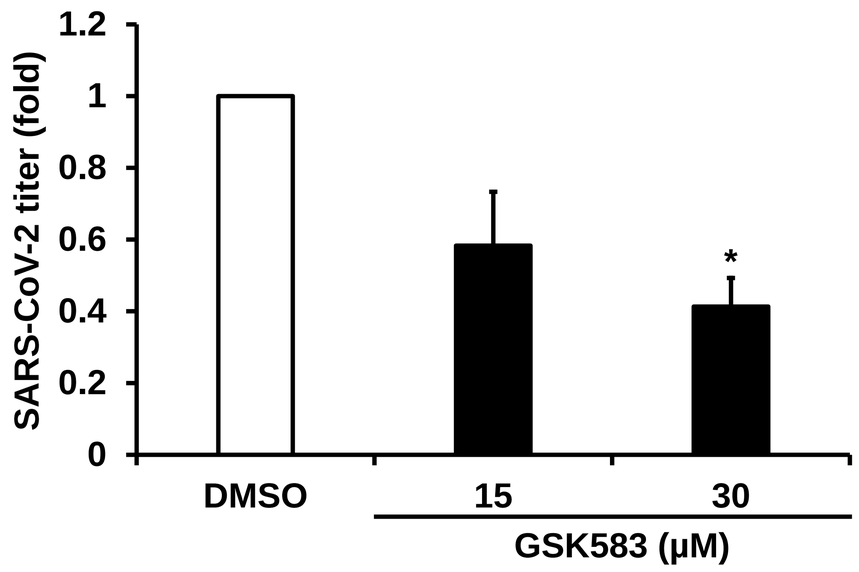
SARS-CoV-2 titer (fold)
1.2
1
0.8
0.6
0.4
0.2
0
*
DMSO
15
30
GSK583 (μM)

B

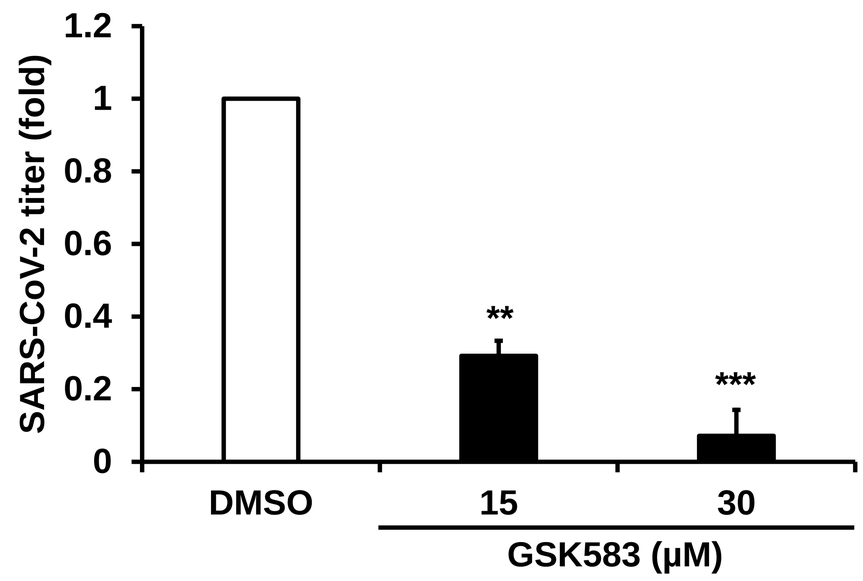
SARS-CoV-2 titer (fold)
1.2
1
0.8
0.6
0.4
0.2
0
**
***
DMSO
15
30
GSK583 (μM)

C

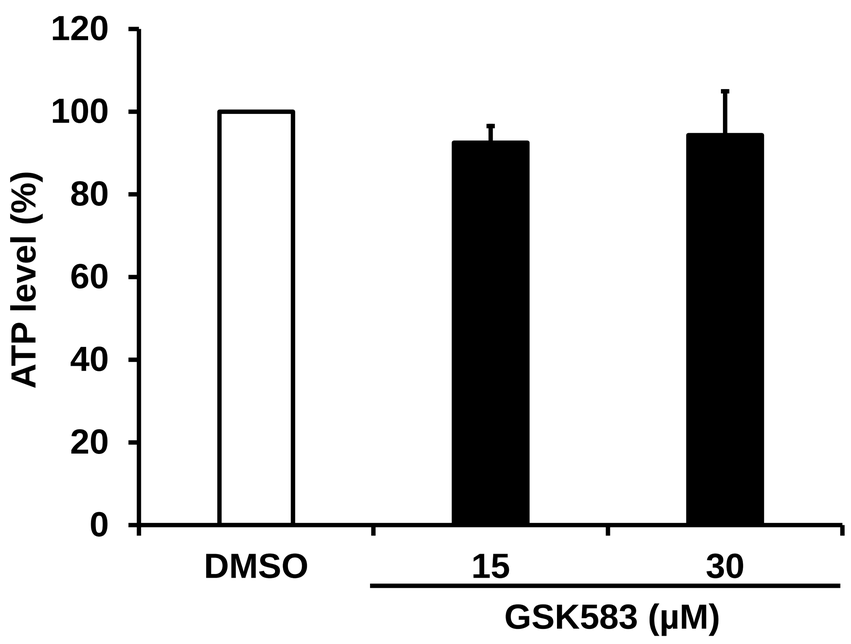
ATP level (%)
120
100
80
60
40
20
0
DMSO
15
30
GSK583 (μM)

D

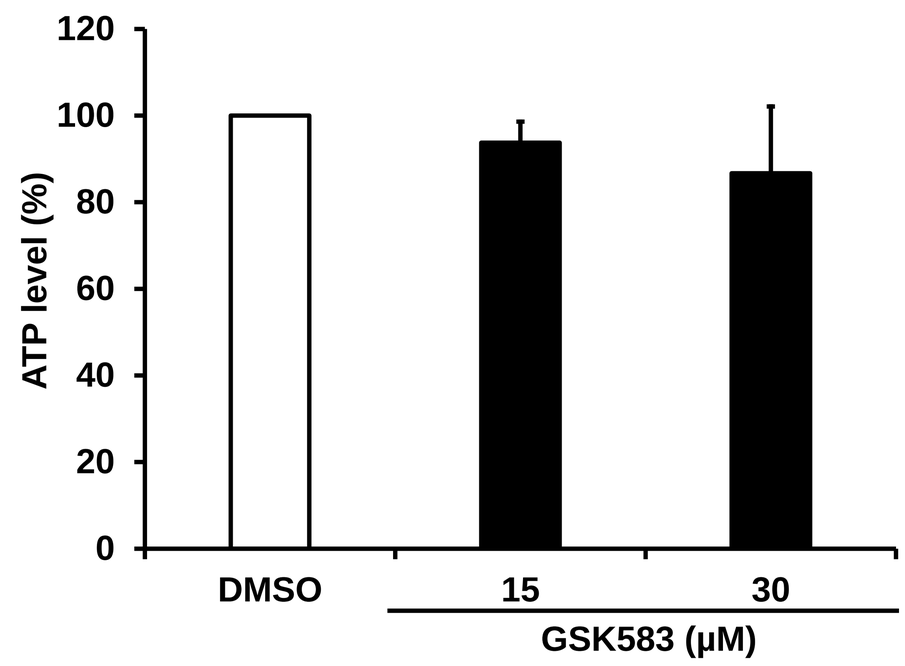
ATP level (%)
120
100
80
60
40
20
0
DMSO
15
30
GSK583 (μM)

E

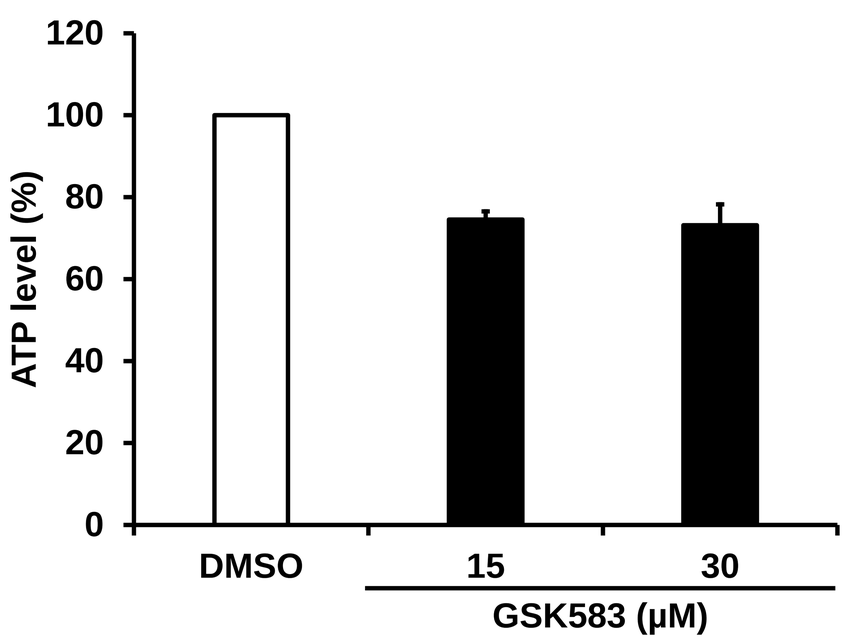
ATP level (%)
120
100
80
60
40
20
0
DMSO
15
30
GSK583 (μM)